Available online at www.sciencedirect.com
SCIENCE DIRECT
Journal of volcanology and geothermal research
ELSEVIER
Journal of Volcanology and Geothermal Research 153 (2006) 221–240
www.elsevier.com/locate/jvolgeores

Melt inclusions from Volcán Popocatépetl and Volcán de Colima, Mexico: Melt evolution due to vapor-saturated crystallization during ascent

Zachary D. Atlas [a,*], Jacqueline E. Dixon [a], Gautam Sen [b], Michael Finny [a], Ana Lillian Martin-Del Pozzo [c]

[a] *University of Miami (RSMAS), 4600 Rickenbacker Causeway. Miami, FL, USA*
[b] *Florida International University, University Park (PC 344). Miami, FL, USA*
[c] *Instituto de Geofisica, Universidad Nacional Autónoma de México (UNAM) Ciudad Universitaria, Circuito Instutos México 04510 Coyoacá, DF, México*

Received 20 April 2004; received in revised form 6 May 2005; accepted 19 June 2005
Available online 19 January 2006

Abstract

Melt inclusions in phenocrysts from Volcán Popocatépetl and Volcán de Colima within the Trans Mexican Volcanic Belt (TMVB) are dacitic to rhyolitic. Trends in melt inclusion major element and water concentrations form the evolved extension of other Mexican volcanics including those presumed to be derived directly from primitive melts. Water concentrations in Popocatépetl and Colima melt inclusions are similar (0.3 to 3.4 wt.% H_2O). Melt-vapor equilibration pressures calculated from dissolved H_2O and CO_2 (Popocatépetl) or H_2O (Colima) in melt inclusions correspond to depths of entrapment of 12 km or less. Water and carbon dioxide concentrations correlate negatively with SiO_2 and potassium. Normalized olivine–augite–quartz compositions are consistent with near cotectic crystallization under vapor-saturated conditions at pressures of 1.5 kb or less. Our results show that Popocatépetl and Colima magmas have undergone vapor-saturated crystallization during ascent in conjunction with varying degrees of mixing between degassed rhyodacitic and less degassed, mafic melts in the upper portions of the crust. These data suggest melt evolution occurred in conduits or inter-fingered dikes rather than a large stratified magma chamber.

Keywords: melt inclusion; volatiles; petrology; Popocatépetl; Colima; México

1. Introduction

Constraining the conditions of crystallization and degassing are critical to understanding volcanic evolution and volcanic hazard. Fractional crystallization in large magma chambers is commonly thought to influence evolution of calc-alkaline magmas in subduction zone settings (Cawthorn et al., 1973; Grove et al., 1982; Grove and Kinzler, 1986; Rutherford and Devine, 1988; Marsh, 1989, 2002; Hervig and Dunbar, 1992; Vaggelli et al., 1993; Sisson and Grove, 1993; Gaetani et al., 1993; Mandeville et al., 1996; Pichavant et al., 2002). Magmatic evolution at some subduction zone volcanoes has also been modeled by polybaric crystallization within several magma chambers at different

* Corresponding author. Tel.: +1 305 361 4810; fax: +1 305 361 4632.
E-mail address: zatlas@rsmas.miami.edu (Z.D. Atlas).

0377-0273/$ - see front matter © 2005 Elsevier B.V. All rights reserved.
doi:10.1016/j.jvolgeores.2005.06.010

depths (Dunbar et al., 1989; Marsh, 1994; Sisson et al., 1996; Grove et al., 1997; Hawkesworth et al., 2000; Rutherford and Devine, 2003). Melt inclusion compositions are representative of the magma in which a given crystal grew, and thus may constrain magmatic history (Roedder, 1979, 1984, 1992; Dunbar and Hervig, 1992; Vaggelli et al., 1993; Nielsen et al., 1995; Vogel and Aines, 1996; Kamenetsky et al., 1997; Lee and Stern, 1998; Gioncada et al., 1998). Total volatile contents of melt inclusions (and all other silicate glasses formed under vapor-saturated conditions) are also useful for constraining the depths of magmatic processes (Sommer, 1977; Roedder, 1984; Webster and Duffield, 1991; Dunbar and Hervig, 1992; Dixon et al., 1995; Dixon and Stolper, 1995; Sisson and Layne, 1996; Dixon, 1997; Moore et al., 1998; Moore and Carmichael, 1998; Roggensack, 2001; Wardell et al., 2001; Newman and Lowenstern, 2002). This study examines melt inclusions from Volcán Popocatépetl and Volcán de Colima, Mexico. We will show that melt inclusion composition is remarkably similar at these two volcanoes and suggests a common evolutionary history in the upper crust. Our data suggest that the melt inclusions from Popocatépetl and Colima are produced by vapor-saturated crystallization during ascent at shallow depth. Mixing between degassed, evolved and less degassed, mafic melts also occurs in the uppermost 12 km. Our work suggests that storage, crystallization and differentiation in a large magma chamber is not required.

2. Geologic setting

Volcán Popocatépetl and Volcán de Colima are large composite volcanoes located within the Trans Mexican Volcanic Belt (TMVB), resulting from subduction of the Cocos and Rivera plates beneath the North American Plate. Popocatépetl is situated in the eastern half of the TMVB approximately 50 km southeast of Mexico City (Fig. 1). Volcán de Colima is located within the Colima graben of western Mexico, approximately 550 km west of Popocatépetl. Volcán Popocatépetl is approximately 350 km from the Middle America Trench while Colima is only 175 km from the trench. Crustal

Fig. 1. Location of Colima and Popocatépetl volcanic complexes in relation to other major eruptive centers along the Trans Mexican Volcanic Belt (tan shadedarea). Inset left shows the Colima volcanic complex and is modified from Luhr and Carmichael (1980). Inset right is for the Popocatépetl-Iztaccihuatl Complex and is modified from Martin Del Pozzo et al. (2003).

thickness has been estimated between 40 and 50 km under Popocatépetl and 30 km under Volcán Colima (Woollard and Monges Caldera, 1956; Wallace and Carmichael, 1999 and references therein; Straub and Martin-Del Pozzo, 2001 and references therein). Both volcanoes are the youngest and southernmost members of local north–south-trending volcanic complexes. Both volcanoes are also the only active members of each group and reflect the trench-ward migration of volcanic activity over time. Both volcanoes experience periods of dome building and collapse. However, eruptions at Popocatépetl are not as regular as those of Colima. The last major eruption of Popocatépetl was approximately 750–1000 y.b.p. (Siebe et al., 1996; Straub and Martin-Del Pozzo, 2001), while Colima has had three major eruptions in the last 2 centuries (Luhr and Carmichael, 1980). Historically, Popocatépetl has had major eruptions every 1000–3000 years (Robin, 1984; Siebe et al., 1996), while Colima has remained nearly continuously active during at least the past 5 centuries (Robin et al., 1987; De La Cruz-Reyna, 1993). Colima's relative proximity to the Middle America Trench may explain its heightened activity as compared to Popocatépetl and other volcanoes of the TMVB (Luhr, 1992).

Popocatépetl and Colima lavas range in composition from mafic andesite to more silicic andesite and dacite (57–64 and 57–66 wt.% SiO_2, MgO 2.4–6.0 and 2.7–4.4 wt.%, respectively) (Luhr and Carmichael, 1980, 1981, 1982, 1990; Robin et al., 1990, 1991; Luhr, 1993). Phenocrysts of plagioclase, orthopyroxene, clinopyroxene and titanomagnetite are prevalent in the lavas of both volcanoes (Luhr and Carmichael, 1990; Luhr and Kyser, 1989; Verma and Luhr, 1993; Robin and Potrel, 1993; Robin et al., 1990; Straub and Martin-Del Pozzo, 2001). At Popocatépetl, olivine phenocrysts occur in lavas from the main edifice. The presence of fosteritic olivine and high Mg # clinopyroxene has been interpreted as an artifact of mixing between mafic and differentiated melts (Boudal and Robin, 1988; Straub and Martin-Del Pozzo, 2001). At Colima, olivine does not occur in lavas from the main vent but does occur from secondary cinder cones along the flanks of the volcano (Luhr and Carmichael, 1981, 1982). Hornblende is also common in Colima lava indicating that these magmas must contain a minimum of 2–4.5 wt.% H_2O (Luhr, 1992; Moore and Carmichael, 1998) and be cooler (Moore and Carmichael, 1998) than their Popocatépetl counterparts.

Studies from Popocatépetl, Colima and other parts of the TMVB have focused on distinguishing between crustal and mantle processes to explain the observed chemical variations in Mexican lavas. Some models require that melt produced in the mantle wedge be modified by crystallization of hydrous minerals (Macías et al., 1993) or by interaction with the lower crust (Verma and Luhr, 1993; Verma, 1999, 2001). Compositions of primitive monogenetic centers such as the Chichinautzan, Zitacuaro-Valle de Bravo and Michoacaun-Guanajato volcanic fields have been used to model source magma compositions (Hasenaka and Carmichael, 1987; Blatter and Carmichael, 1998; Wallace and Carmichael, 1999; Chesley et al., 2002; Carmichael, 2002). Recent studies of melt inclusions from more primitive volcanoes such as Xitle (Cervantes and Wallace, 2003) and Paricutin (Luhr, 2001) have been used to estimate volatiles in the source region. Other studies have modeled the variety of magmatic compositions as products of simple differentiation due to crystal fractionation (Righter and Carmichael, 1996) or combined fractionation, mixing and assimilation (Allan and Carmichael, 1984; Hasenaka and Carmichael, 1987; Wallace and Carmichael, 1994). While a number of these studies have been used to define source characteristics (see Carmichael, 2002 and references therein), nearly all studies have agreed that many of these melts have been fractionated at low (crustal) pressures (Hasenaka and Carmichael, 1987; Robin and Potrel, 1993; Righter and Carmichael, 1996; Blatter and Carmichael, 1998; Moore and Carmichael, 1998; Wallace and Carmichael, 1999; Blatter and Carmichael, 2001; Martin Del Pozzo et al., 2003).

3. Methods

3.1. Sample preparation

Bulk samples from Popocatépetl and Colima were collected from lava flows and pyroclastic eruptions. Air fall deposits from Popocatépetl were collected by A. L. Martin Del Pozzo and H. Delgado (UNAM) during the eruptive period of 1994–1998 and sampling location are those shown in Martin-Del Pozzo et al. (2002). Sample locations for Colima are given by Luhr and Carmichael (1990) and also include 2 lava samples from Thomas and Draper (1991 field study). Sample DI-194 is from the lava flow of the *Volcancito* near the base of the "Plyon" adjacent to the caldera wall on the northeast flank of Fuego de Colima. Sample JT 91-68 was collected from the base of the 1890 flow nearest to the caldera wall (adjacent to the 1913 deposit).

Bulk samples were cut into thin sections and inspected visually for melt inclusions. Samples were

then hand crushed and mineral separates of plagioclase, orthopyroxene, clinopyroxene and hornblende were collected for analysis. Although olivine is present at Popocatépetl and is a preferred mineral to use in melt inclusion studies because of its hardness and lack multiple cleavages (USGS Melt Inclusion Web Page, Lowenstern), optical analysis did not reveal melt inclusions in olivine.

Mineral grains of plagioclase, orthopyroxene and clinopyroxene from Popocatépetl were prepared for FTIR analysis using methods modified from Dixon and Clague (2001), Gioncada et al. (1998), and Vogel and Aines (1996). A second set of Popocatépetl melt inclusions were polished on one side and mounted aluminum disks with Buehler Epoxide resin for SIMS analysis (Hauri, personal communication). Popocatépetl melt inclusions were found to be vitreous and free of secondary phases (except for a vapor bubble) and did not require re-homogenization.

Mineral separates for Colima lava were extracted from the crushed bulk rock using a Frantz Magnetic separator, mounted on a glass slide using petropoxy and polished on one side only. Analyses on Colima melt inclusions were also preformed on whole rock sections polished to expose a single melt inclusion. Because many of the melt inclusions found in plagioclase from Colima were devitrified or contained secondary phases, a series of experiments were performed to re-homogenize the melt inclusions and determine the temperature of vitrification. These experiments were performed in a 1 atm tube furnace using methods similar to Sinton et al. (1993) and Dunbar and Hervig (1992) after Nielsen et al. (1995). Temperature was calibrated on pure diopside using an internal $Pt–Rh_{5\%}$ thermocouple and external, Oxytrol Systems reference thermocouple and was accurate to within ± 1 °C. Oxygen fugacity was controlled by a mixture of CO_2 and H_2 gas to approximately +1 log units above the NNO buffer to approximate the fO_2 conditions reported for Colima (Luhr and Carmichael, 1980). Re-homogenization runs were kept to less than 45 min duration to limit migration of volatile species (e.g., H_2O, CO_2 and Na_2O) (Nielsen et al., 1998). Samples were drop quenched in distilled water (<0.5 s) to ensure no growth of secondary crystals. Re-homogenized inclusions were optically clear and typically contained one or two vapor bubbles.

3.2. EPMA analysis

Major elements were analyzed using an electron probe micro analyzer (EPMA) at Florida International University. Colima melt inclusions were analyzed on a JEOL 8900R EPMA while melt inclusions from Popocatépetl were analyzed on an ARL SEMQ EPMA. Information on nine elements was gathered for Colima melt inclusions, while 10 element analyses were preformed on Popocatépetl melt inclusions. Analytical conditions for Colima melt inclusions were 15 kV accelerating potential and 20 nA beam current. Analytical conditions on the ARL SEMQ were 15 kV and 25 nA. Many of the melt inclusions were smaller than 25 μm, therefore they were analyzed with ≤3 μm beam to ensure that there was no overlap with the host crystal and that analyses could be reproduced if necessary. Although such conditions generally result in volatile loss (e.g., loss of sodium, with lesser loss of potassium), they were chosen because they represent the best analytical conditions for geologic material and provide statistically meaningful count rates (Nielsen and Sigurdsson, 1981). However, it was necessary to keep the counting times short (<10 s per element) to limit sodium loss and gain of other elements (e.g., "ingrowth" of Al and Si, Morgan and London, 1996). Standard accuracy on each element was less than 2% for basaltic glass standard (BHVO) and was <5% for elements in rhyolitic glass (SPI-2 obsidian glass) with concentrations over 1 wt.% (Table 1). Despite good internal consistency ($\sigma \leq 0.555$), accuracy based on standard compositions versus published values was poor (up to ±68%) for elements with concentrations below 1 wt.% in the rhyolitic glass.

Sodium was always gathered during the first pass and analyzed for no more than 10 s. No more than a 30 s analysis was performed on any other element and most analyses were kept to 10 s. It has been shown that the sodium loss can be estimated and corrected at these conditions (provided that count times are kept short enough for there to be negligible loss of potassium) using a "time zero" correction based on sodium decay curves (Devine et al., 1995; Nielsen and Sigurdsson, 1981). Since all microprobes are not the same we have generated our own decay curves in order to correct for sodium loss. For this we used a rhyolite glass (SPI-2 obsidian glass) containing 0.8 wt.% H_2O and have determined that sodium loss was as high as 40% during the first 10 s of analysis. Correction of standard values using this method reduces the error to 1.12% (from ~30%) for the rhyolite standard (Table 1). We have assumed that our samples have incurred a similar loss (although this loss may be somewhat higher in the more hydrous samples, see Morgan and London, 1996) and sodium has been corrected accordingly.

Table 1
Standard calibrations and calculated errors

Standard calibration for EPMA Analysis									
Microprobe analysis of SPI-2 obsidian					Microprobe analysis of BHVO				
	Average[a]	SD	Published values	%Diff[b]		Average[c]	SD	Published values	%Diff[b]
SiO_2	75.814	0.555	73.940	2.53	SiO_2	49.741	0.707	49.580	0.33
TiO_2	0.064	0.022	0.100	35.81	TiO_2	2.738	0.053	2.740	0.09
Al_2O_3	12.855	0.080	13.110	1.94	Al_2O_3	13.589	0.150	13.610	0.16
FeO	1.732	0.108	1.720	0.72	FeO	10.939	0.137	10.930	0.09
MnO	0.070	0.014	0.060	17.46	MnO	0.167	0.032	0.170	1.85
MgO	0.022	0.012	0.070	68.57	MgO	7.051	0.158	7.090	0.56
CaO	0.709	0.028	0.760	6.74	CaO	11.341	0.131	11.350	0.08
Na_2O	2.868	0.093	4.060	29.37	Na_2O	2.397	0.111	2.400	0.11
Ctd Na_2O[d]	4.015	0.130	4.060	1.12	K_2O	0.510	0.031	0.520	1.86
K_2O	5.046	0.067	5.040	0.11	P_2O_5	0.267	0.029	0.270	1.01
Total	99.181	0.486	98.860	3.63	Total	98.741	0.755	98.660	0.08

[a] $N=21$.
[b] % Difference = absolute value of (standard − unknown/standard) * 100.
[c] $N=61$.
[d] Ctd Na_2O=corrected Na_2O determined from Na decay curve loss at $t=10$ s for 20 nA and <3 μm beam diameter.

3.3. FTIR analysis

FTIR measurements for CO_2 and H_2O were made using the microscope attachment to the Brüker IFS66 infrared spectrometer at the University of Miami for Popocatepétl only. Because of their small size, no attempt was made to analyze Colima melt inclusions using FTIR. We employed methods similar to Dixon and Clague (2001). Total dissolved water was measured using the fundamental OH^- stretching band at 3550 cm^{-1}. CO_2 dissolved as molecular CO_2 (2250 cm^{-1}) and carbonate groups (1515 and 1430 cm^{-1}) was not detected. To eliminate the effect of overlap of the IR beam with the host mineral, the spectrum of the host mineral was subtracted from the melt inclusion spectrum. Absorbances were converted to weight percent H_2O using the Beer–Lambert law: $C_i = 100\ (MW_i \cdot A / d\rho)$; where: C_i=species concentration (wt.%), MW_i is the molecular weight of the volatile species (g/mol; 18.015 for H_2O), A is the absorbance (absorbance units), d is the sample thickness (cm), ρ is glass density (g/l) and is the molar absorptivity (L/mol · cm). Absorbance and molar absorptivity were calculated using a straight-line background correction (after Dixon et al., 1995). Glass densities were calculated based on melt composition, using the Gladstone–Dale rule and the Church–Johnson equation as described by Silver et al. (1990). Molar absorptivity values for water are 62.3 ± 0.4 L/mol · cm for andesite (Mandeville et al., 2002), 68 ± 5 L/mol · cm for dacite (Yamashita et al., 1997) and $90 + 10$ L/mol · cm for rhyolite (Hauri et al., 2002). Analysis of a variety of rhyolitic standard glasses results in water concentrations within 5% of accepted values (see Hauri et al., 2002). Precision of measurement was better than 5%. Melt inclusion thickness was estimated assuming a uniform shape. Round inclusions were assumed to be spherical and elongate inclusions ellipsoidal. Thickness was estimated to be the minor axis in the case of ellipsoid inclusions. Application of such estimates produces up to a 50% uncertainty in the FTIR measurement of water concentration, significantly higher than the SIMS analysis.

3.4. Secondary Ion Mass Spectrometry (SIMS) analysis

Water and CO_2 in Popocatépetl melt inclusions were measured using a Cameca 6f SIMS at the Department of Terrestrial Magnetism, Carnegie Institute of Washington following the procedures of Hauri et al. (2002). The primary Cs^+ beam was used with a current of 5–10 nA and 10 kV accelerating potential using ^{30}Si as an internal standard. Analytical uncertainty is <10% for trace elements, ± 10% for H_2O, and ± 15% for CO_2 (Hauri et al., 2002).

Colima melt inclusions were analyzed for water and trace elements but not CO_2 using the Cameca 3f SIMS at Arizona State University. Analytical conditions for the SIMS were −12.55 kV primary accelerating voltage, 4500 V secondary accelerating voltage using a O^- primary ion beam with an arc current fixed at 80 mA. A 75 V offset was used to limit molecular interference of oxygen ions (Hervig et al., 1989; Hervig and Dunbar, 1992; Dunbar and Hervig, 1992). Calibration techniques for hydrogen (and subsequently water) were iden-

tical to those described by Ihinger et al. (1994). The data (collected as total hydrogen on the SIMS) were converted to total water content following Ihinger et al. (1994). Analytical uncertainty was ±10% for H_2O (Ihinger et al., 1994).

4. Results

4.1. Major element trends

Major element concentrations from Popocatépetl and Colima melt inclusions are similar (Fig. 2). Most melt inclusions are dacitic to rhyolitic in composition. Silica contents in Popocatépetl and Colima melt inclusions range from 60 to 77 wt.%; however, two are basaltic andesitic (SiO_2 55–56 wt.%) and one is very high in silica (~80 wt.% SiO_2) (Table 2). The inclusions are generally more differentiated than the bulk rock, which is andesitic in composition (Luhr and Carmichael, 1980, 1981, 1982, 1990; Robin et al., 1990; Robin and Potrel, 1993) and are similar to the highly differentiated pumices at Popocatépetl (Straub and Martin-Del Pozzo, 2001). Colima melt inclusions are also generally more differentiated than experimental glasses produced from low-pressure crystallization experiments (Moore and Carmichael, 1998). Trends in major element composition are consistent with differentiation due to crystallization of the typical Popocatépetl and Colima assemblage (plagioclase, clinopyroxene, orthopyroxene, Ti-magnetite, ± olivine, ± hornblende) (Luhr and Carmichael, 1980; Straub and Martin-Del Pozzo, 2001). MgO concentration is typically low (0.0–2.5 wt.%) in

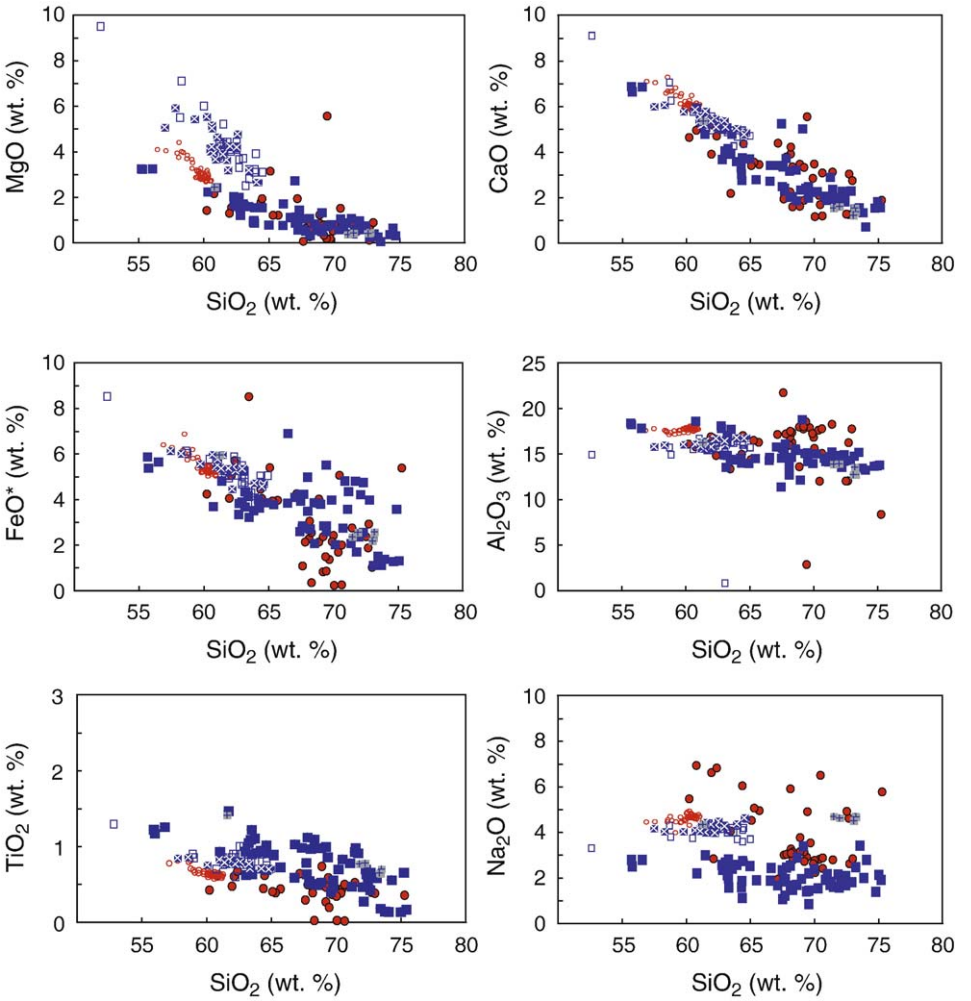

Fig. 2. Melt inclusions and bulk rock compositions for V. Popocatépetl and V. Colima. Symbols are as follows: (■) Popocatépetl MI's, (●)Colima MI's, (○) Colima lava (Luhr and Carmichael, 1990), (□) Popocatépetllava (Boudal and Robin, 1988), (⊠) Popocatépetl tephra and (⊞) Popocatépetl pumice (Straub and Martin-Del Pozzo, 2001).

Table 2
Major element analyses for Popocatépetl and Colima melt inclusions

EPMA Analysis of Popocatépetl melt inclusions in natural samples from 1994 to 1998 (concentrations in wt.%)

Sample[a]	Host	Date	SiO_2	TiO_2	Al_2O_3	MnO	MgO	FeO	CaO	Na_2O[b]	K_2O	P_2O_5	Total
AMEC 2A	cpx	8/29/98	70.807	0.784	14.559	0.039	0.574	2.750	1.896	1.067	2.726	0.132	95.334
AMEC 2B	cpx		72.383	0.662	14.930	0.032	0.582	2.566	2.010	0.925	2.144	0.120	96.355
AMEC 2C	cpx		72.090	0.639	14.377	0.045	0.537	2.438	1.839	0.936	2.705	0.115	95.722
AMEC 2D	cpx		72.016	0.701	14.129	0.048	0.517	2.360	1.714	0.983	2.752	0.108	95.327
AMEC 4A	cpx		67.441	0.787	11.368	0.038	2.711	4.248	5.076	1.305	1.996	0.167	95.136
AMEC 10A	plag		81.352	0.116	10.557	0.028	0.014	0.364	0.313	1.919	5.876	0.014	100.549
AMEC 13A	plag		74.019	0.560	13.245	0.014	0.061	1.378	0.537	1.563	4.172	0.064	95.611
AMEC 14A	plag		68.602	0.530	15.380	0.023	0.322	2.077	1.697	1.620	3.017	0.068	93.335
ATLA-1A	cpx	10/29/96	63.168	1.091	13.532	0.106	1.994	5.257	4.897	1.180	0.953	0.532	92.709
ATLA-1B	cpx		64.926	0.883	13.950	0.072	1.541	3.858	3.528	1.409	1.980	0.324	92.473
ATLA-1C	cpx		63.910	0.952	14.349	0.046	1.584	3.520	3.413	1.436	2.064	0.342	91.615
ATLA-1D	cpx		64.355	1.023	14.001	0.053	1.541	3.818	3.574	1.535	1.938	0.322	92.160
ATLA-1E	cpx		63.477	1.111	14.430	0.049	1.710	4.144	3.776	1.406	1.627	0.337	92.066
ATLA-1F	cpx		62.997	1.053	14.884	0.071	1.612	3.906	3.874	1.495	1.749	0.322	91.962
ATLA-1G	cpx		63.239	1.225	14.837	0.045	1.530	4.363	3.727	1.566	1.941	0.363	92.835
ATLA-2A	cpx		67.546	1.122	15.616	0.057	1.140	3.944	3.175	1.029	2.244	0.262	96.135
ATLA-2B	cpx		68.562	0.980	15.560	0.030	1.064	3.862	3.051	0.946	2.357	0.238	96.647
ATLA-2C	cpx		67.091	0.986	15.782	0.057	1.112	4.108	3.243	0.927	2.446	0.273	96.023
ATLA-4B	opx		64.297	0.931	14.411	0.066	0.980	3.810	2.866	1.037	1.908	0.226	90.532
ATLA-4C	opx		64.258	0.705	14.540	0.060	0.922	4.020	3.151	0.884	2.070	0.262	90.871
ATLA-8A	opx		65.455	0.731	14.508	0.077	0.785	3.782	2.617	1.050	1.608	0.156	90.769
ATLA-8B	opx		68.078	0.511	13.590	0.057	0.572	3.498	1.845	0.922	1.632	0.106	90.811
ATLA-8C	opx		66.527	0.594	14.277	0.070	0.771	3.856	2.550	1.040	1.700	0.204	91.588
ATLA-8D	opx		64.340	0.690	14.330	0.050	0.860	3.630	2.590	0.612	1.340	0.180	88.622
TETEL-1A	opx	6/30/97	55.698	1.229	18.361	0.095	3.238	5.886	6.701	1.561	1.371	0.293	94.435
TETEL-1B	opx		56.548	1.259	17.814	0.083	3.246	5.658	6.688	1.559	1.070	0.302	94.227
TETEL-1C	opx		61.442	1.470	16.136	0.096	2.420	4.825	4.608	1.673	1.665	0.358	94.691
TETEL-1D	opx		55.773	1.174	18.205	0.095	3.227	5.381	6.469	1.393	1.057	0.298	93.071
TETEL-4A	opx		63.554	0.918	17.706	0.042	1.622	3.228	4.606	1.343	1.569	0.297	94.884
TETEL-4B	opx		62.755	0.939	18.085	0.053	2.034	3.350	4.837	1.436	1.764	0.276	95.530
TETEL-4C	opx		60.796	0.937	18.606	0.023	2.223	3.697	5.759	1.222	1.511	0.243	95.017
TETEL-5A	cpx		63.276	0.635	17.009	0.044	1.206	4.338	3.778	0.873	1.389	0.288	92.835
TETEL-6A	opx		71.781	0.467	14.514	0.083	1.060	4.811	1.714	1.201	2.369	0.099	98.097
TETEL-6B	opx		69.515	0.556	14.152	0.106	1.315	5.522	2.234	1.226	2.251	0.368	97.246
TETEL-6C	opx		70.954	0.474	14.190	0.086	1.041	4.819	1.714	1.207	2.463	0.048	96.995
TETEL-6D	opx		72.375	0.426	14.194	0.061	0.969	4.759	1.648	1.164	2.575	0.075	98.245
TETEL-6E	opx		66.565	1.030	14.617	0.124	1.709	6.912	3.240	1.363	2.248	0.613	98.422
TETEL-7A	opx		68.953	0.999	12.147	0.049	0.837	3.856	2.167	1.089	2.498	0.192	92.784
TETEL-7B	opx		68.077	1.100	12.711	0.037	1.045	4.993	2.986	1.414	2.329	0.288	94.976
TETEL-9A	opx		63.239	0.898	16.927	0.080	1.658	3.677	3.983	1.097	1.734	0.297	93.587
TETEL-9B	opx		62.797	0.628	17.790	0.030	1.680	3.829	3.504	1.306	1.635	0.314	93.513
TETEL-10A	opx	6/30/97	69.519	0.458	14.615	0.070	0.486	2.597	1.819	0.463	1.688	0.087	91.801
TETEL-10B	opx		68.263	0.492	14.635	0.031	0.509	2.707	1.877	0.815	2.118	0.060	91.507
TETEL-10C	opx		67.683	0.526	14.997	0.076	0.561	2.844	2.114	1.085	2.056	0.112	92.050
TETEL-10D	opx		69.332	0.404	15.035	0.050	0.541	2.845	2.252	0.783	1.990	0.055	93.288
TETEL-10E	opx		69.529	0.474	15.125	0.039	0.594	2.850	2.322	0.797	1.819	0.095	93.644
TETEL-12A	opx		74.961	0.659	13.679	0.055	0.638	3.572	1.646	1.192	3.051	0.108	99.558
TETEL-12B	opx		69.095	0.863	18.760	0.042	0.706	3.801	4.847	1.893	1.344	0.275	101.625
TETEL-12C	opx		69.924	0.700	13.969	0.050	0.717	3.977	2.064	1.336	2.883	0.277	95.898
TETEL-12D	opx		67.782	0.970	16.084	0.081	1.446	4.238	3.542	1.368	2.262	0.222	97.995
TETEL-13E	Plag		73.799	0.139	13.462	0.029	0.261	1.118	1.179	1.112	2.137	0.073	93.309
TETEL-13I	Plag		75.157	0.172	13.781	0.041	0.303	1.315	1.389	1.065	2.497	0.065	95.785

(continued on next page)

Table 2 (*continued*)

Sample[a]	Host	Date	SiO_2	TiO_2	Al_2O_3	MnO	MgO	FeO	CaO	Na_2O[b]	K_2O	P_2O_5	Total
TETEL-14A	Plag		73.509	0.146	15.174	0.047	0.392	1.511	1.381	1.915	3.062	0.117	97.252
TETEL-14B	Plag		73.166	0.182	14.730	0.080	0.234	1.109	1.342	1.378	2.697	0.117	95.036
TETEL-15A	Plag		71.863	0.277	14.838	0.029	0.393	1.698	1.808	0.870	2.149	0.016	93.942
TETEL-16A	Plag		67.669	0.547	14.603	0.041	0.886	2.748	2.239	0.674	1.698	0.183	91.289
TETEL-16C	Plag		67.475	0.637	14.534	0.052	0.863	2.596	2.314	0.587	1.657	0.196	90.909
TETEL-17A	Plag		74.724	0.138	13.666	0.022	0.352	1.278	1.365	0.773	2.015	0.070	94.399
CHOL-2A	Pig	5/11/97	72.862	0.587	14.283	0.062	0.740	3.983	2.124	1.009	2.750	0.177	98.575
CHOL-2B	Pig		71.236	0.982	14.718	0.045	0.889	4.365	2.718	1.012	2.457	0.242	98.664
CHOL-2C	Pig		71.177	0.933	14.121	0.042	0.651	3.572	1.768	0.940	3.086	0.142	96.432
CHOL-2D	Pig		72.180	0.556	13.546	0.101	0.606	4.227	2.119	1.141	2.852	0.198	97.525
CHOL-4A	opx		71.427	0.914	15.193	0.030	0.872	2.080	2.189	0.895	2.331	0.127	96.057
CHOL-4B	opx		70.224	0.832	14.998	0.038	0.792	2.030	2.101	0.853	2.298	0.099	94.265

[a]Sample names are as follows: AMEC=Amecameca, ATLA=Atlixco, TETEL=Tetela del Volcán, Chol=Cholula. Sampling locations are given in Martin-Del Pozzo et al. (2002).

[b]Indicates pre-corrected values for sodium. Sodium values for figures were corrected using "zero-back" correction method from Devine et al. (1995), Nielsen and Sigurdsson (1981).

EPMA Analysis of Colima melt inclusions in natural samples from 1869 to 1913 (concentrations in wt.%)

Sample[a]	SiO_2	TiO_2	Al_2O_3	FeO*	MnO	MgO	CaO	Na_2O	K_2O	Total	n[b]
Melt inclusion analysis—1004-421 (1913)											
1004-421PLAG-MI1	75.270	0.357	8.377	5.390	0.092	1.617	1.891	4.430	0.211	97.635	3
1004-421PLAG-MI2	63.470	1.080	13.390	8.530	0.160	2.590	2.190	2.720	1.630	95.760	1
1004-421CPX-MI1	70.050	0.026	15.628	0.236	0.021	0.020	1.166	0.890	1.184	89.221	5
1004-421CPX-MI2	70.635	0.017	15.080	0.260	0.014	0.000	1.198	1.073	1.370	89.646	2
1004-421HBL-MI	68.300	0.025	16.300	0.356	0.032	-	1.600	1.430	1.570	89.614	1
Melt inclusion analysis—M82-11 (1890)											
M82-11PLAG-MI-1	70.465	0.447	12.020	5.070	0.138	1.519	1.690	5.160	4.275	100.783	2
M82-11OPX-MI-1	70.367	0.387	17.627	1.693	0.068	0.652	2.100	1.469	1.797	96.160	3
M82-11OPX-MI-2	69.680	0.370	17.910	1.370	0.052	0.188	2.200	2.190	2.870	96.829	2
Melt inclusion analysis—91-68 (1913?)											
91-68PLAG-MI-1	61.380	0.089	21.790	1.205	0.016	0.157	4.530	9.710	1.300	100.177	1
91-68OPX-MI-1	69.388	0.589	18.555	1.496	0.050	0.198	2.438	1.568	2.065	96.345	4
91-68HBL-MI-1	67.610	0.296	21.750	1.088	0.041	0.070	1.940	1.660	1.850	96.305	1
Melt inclusion analysis—1004-414 (1869)											
1004-414PLAG-MI1	60.400	0.568	17.550	4.720	0.170	1.469	4.100	10.240	2.140	101.398	1
1004-414PLAG-MI2	61.770	0.693	15.687	4.866	0.104	2.071	4.650	8.147	1.897	99.885	3
1004-414CPX-MI-1	69.190	0.270	17.780	0.834	0.033	0.340	1.880	1.800	1.680	93.808	1
1004-414HBL-MI	69.450	0.195	2.880	0.860	0.007	5.570	5.555	3.560	0.473	88.549	2

[a]Samples 1004-421, M82-11, 91-68 and 1004-414 collected by J. F. Luhr. Sample locations, lava composition and crystallinity are given in Luhr and Carmichael (1980, 1981, 1982, 1990).

[b]n equals the number of analyses taken on individual melt inclusions (see supplemental data table for individual analyses and standard deviation).

EPMA analysis of melt inclusions in plagioclase from Volcán Colima. Analyses are for controlled fugacity re-homogenization experiments on sample DI-194 (1869) (concentrations in wt.%).

Sample[a]	SiO_2	TiO_2	Al_2O_3	FeO*	MnO	MgO	CaO	Na_2O	K_2O	Total	n[b]
Melt inclusion analysis for controlled fO_2 run at 1150 °C											
DI194CF1b.2a	60.220	0.426	16.110	4.250	0.088	1.427	4.650	4.130	1.700	93.001	1
DI194CF1b.2b	65.700	0.441	16.310	3.970	0.064	1.213	3.460	3.610	1.900	96.668	1
DI194CF1b.2c	65.300	0.390	16.510	3.940	0.046	1.218	3.560	3.720	1.835	96.518	2
DI194CF1b.2d	62.120	0.607	16.780	5.055	0.096	1.551	5.180	1.459	1.238	94.086	2
DI194CF1b.2e	61.960	0.475	16.910	4.060	0.076	1.299	3.910	5.280	1.480	95.451	1

Table 2 (*continued*)

Sample[a]	SiO_2	TiO_2	Al_2O_3	FeO*	MnO	MgO	CaO	Na_2O	K_2O	Total	n[b]
Melt inclusion analysis for controlled fO_2 run at 1140 °C											
DI194CF2.1a	68.120	0.512	15.960	2.290	0.029	0.277	2.250	4.570	2.620	96.629	1
DI194CF2.1c	72.680	0.441	12.060	1.880	0.045	0.121	1.264	3.720	2.330	94.541	1
Melt inclusion analysis for controlled fO_2 run at 1130 °C											
DI194CF3.1a	65.088	0.405	14.398	5.405	0.142	3.151	3.410	3.183	1.950	97.131	4
DI194CF3.2b	68.880	0.739	13.623	4.030	0.072	1.233	1.620	2.430	3.020	95.647	3
DI194CF3.2c	72.523	0.571	12.053	2.377	0.043	0.759	1.280	3.583	2.867	96.057	3
Melt inclusion analysis for controlled fO_2 run at 1120 °C											
DI194CF4.1a	61.920	0.522	16.010	4.770	0.070	1.680	4.870	6.245	1.555	97.641	2
DI194CF4.1b	62.370	0.677	14.860	5.720	0.112	1.980	4.710	5.030	1.830	97.289	1
DI194CF4.1c	64.365	0.447	14.990	4.460	0.099	1.790	3.720	4.700	1.765	96.335	2
DI194CF4.1d	60.775	0.618	15.795	5.425	0.097	2.165	4.960	5.595	1.425	96.855	2

[a]Sample DI-194 collected by J. Thomas and G. Draper in 1991 field study (unpublished).
[b]*n* equals the number of analyses taken on individual melt inclusions (see supplemental data table for individual analyses, standard deviation and modal crystallinity).

Popocatépetl and Colima melt inclusions. CaO is also low, with concentrations ranging from 0.5 to 6.0 wt.%. Both MgO and CaO correlate negatively with SiO_2. FeO* concentrations (0–6 wt.%) also correlate negatively with SiO_2. Al_2O_3 concentrations define a fairly flat trend except at high SiO_2 (>63%) where they decrease slightly, consistent with late stage plagioclase crystallization. To some extent Na_2O behaves similar to Al_2O_3. However, despite our correction for loss during measurement, Na_2O concentrations in Popocatépetl melt inclusions are lower than expected. Na_2O concentrations in Colima melt inclusions show considerably less Na loss during analysis but are still widely scattered. In general, rehomogenized melt inclusions have higher and more consistent values of Na_2O than un-homogenized melt inclusions. A line scan analysis across a melt inclusion in plagioclase shows that additional loss of Na may have been due in part to post entrapment crystallization of sodic plagioclase along the walls of the inclusion (Fig. 3). K_2O concentrations correlate positively with SiO_2 (Fig. 4). While compatible major elements should decrease with increasing SiO_2, incompatible elements will have the opposite trend. For the typical crystallizing assemblage of both Popocatépetl and Colima we would expect potassium to behave incompatibly during differentiation due to crystallization and therefore potassium is our best indicator of degree of differentiation.

4.2. H_2O and CO_2 in melt inclusions

H_2O and CO_2 were analyzed in 45 Popocatépetl melt inclusions. Water was measured in four Volcán de Colima melt inclusions (Table 3). Water from Popocatépetl measured by FTIR ranges from 1.10 ± 0.09 to

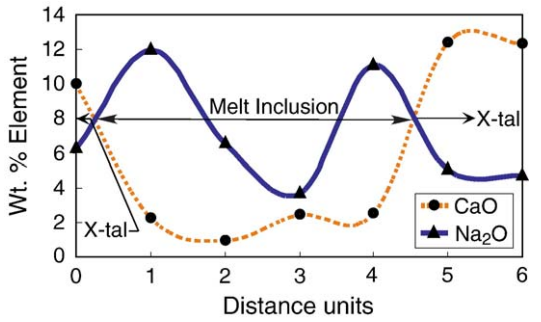

Fig. 3. Profile of CaO and Na_2O along a transect across a melt inclusion hosted in plagioclase from un-homogenized sample M82-11 (Volcan Colima). Sodium spikes are evident along the rims of the melt inclusion. Each distance measurement is approximately 5 to 10 μm.

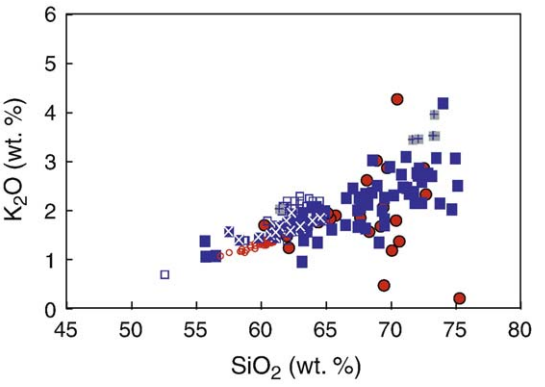

Fig. 4. Plot of SiO_2 vs. K_2O for Colima and Popocatépetl melt inclusions. Colima Lavas (Luhr and Carmichael, 1990) and Popocatépetl lavas, tephras and pumace (Straub and Martin-Del Pozzo, 2001; Boudal and Robin, 1988) are plotted for comparison. Symbols are the same as in Fig. 2.

Table 3
Water and CO_2 contents for Popocatépetl and Colima melt inclusions

Sample	Host crystal	H_2O (wt.%) (FTIR)	H_2O (wt.%) (SIMS)	CO_2 (ppm)[a]	Entrapment pressure (bars)[b]
Popocatépetl					
AMEC 2A	cpx	–	1.47	433	1098
AMEC 2B	cpx	–	1.52	939	2116
AMEC 2C	cpx	1.24	1.32	840	1860
AMEC 4A	cpx	–	1.73	322	962
ATLA-1A	cpx	–	1.89	472	1319
ATLA-1B	cpx	–	1.59	519	1308
ATLA-1C	cpx	1.98	1.63	537	1357
ATLA-1D	cpx	–	1.68	352	1005
ATLA-1E	cpx	1.66	1.82	834	2012
ATLA-1F	cpx	1.72	1.80	1288	2889
ATLA-1G	cpx	–	1.57	1458	3139
ATLA-2A	cpx	–	1.53	1394	3004
ATLA-8A	opx	–	2.03	580	1587
ATLA-8B	opx	–	2.12	587	1636
ATLA-8C	opx	–	2.07	466	1375
ATLA-8D	opx	–	3.02	1045	2909
TETEL-1A	opx	–	2.07	470	1383
TETEL-1B	opx	1.71	1.76	639	1605
TETEL-4A	opx	–	1.85	402	1164
TETEL-4B	opx	–	1.37	595	1390
TETEL-4C	opx	–	1.68	649	1597
TETEL-5A	cpx	2.26	2.29	622	1773
TETEL-6A	opx	1.32	1.53	351	953
TETEL-6B	opx	2.04	1.52	436	1120
TETEL-6C	opx	1.57	1.39	268	745
TETEL-6D	opx	1.67	1.35	322	840
TETEL-6E	opx	1.69	1.60	401	1076
TETEL-7A	opx	–	1.27	453	1078
TETEL-7B	opx	–	1.40	469	1148
TETEL-9A	opx	–	2.67	843	2367
TETEL-10A	opx	1.41	2.09	484	1419
TETEL-10B	opx	–	1.73	240	798
TETEL-10C	opx	1.04	2.17	643	1767
TETEL-10D	opx	0.83	2.12	314	1090
TETEL-10E	opx	1.98	1.97	397	1199
TETEL-12C	opx	–	1.35	866	1920
TETEL-13E	Plag	1.90	–	–	n/a
TETEL-14A	Plag	1.10	–	–	n/a
TETEL-14B	Plag	2.10	–	–	n/a
TETEL-15A	Plag	1.88	–	–	n/a
TETEL-16A	Plag	1.73	–	–	n/a
TETEL-16C	Plag	2.97	–	–	n/a
TETEL-17	Plag	2.09	–	–	n/a
CHOL-2B	opx	–	0.8	102	273
CHOL-4A	opx	–	1.95	380	1157
Fuego de Colima					
1004-414 MI1	Plag	–	0.394	–	n/a
M82-11 MI 2	opx	–	0.716	–	n/a
1004-421 MI 1	cpx	–	3.420	–	n/a
1004-421 MI 2	cpx	–	2.760	–	n/a

[a] CO_2 concentrations from SIMS analyses only. FTIR showed baseline concentrations of CO_2 in all samples tested.

[b] Entrapment pressures are calculated from VolatileCalc (Newman and Lowenstern, 2002) and reflect saturation for rhyolite melt at 1050 °C.

2.97 ± 0.50 wt.%. Water contents obtained using SIMS range from 0.80 ± 0.07 to 3.02 ± 0.30 wt.% and are in agreement with the FTIR data within uncertainties. Thus, despite our concern for possible large uncertainties in inclusion thickness, our IR data appear to give quantitatively useful estimates.

At Colima, pyroxene hosted melt inclusions from the 1913 scoria (samples 1004-421-PXMI-1 and 1004-421-PXMI-2) are the most water-rich and contain 3.4 ± 0.3 and 2.8 ± 0.3 wt.% H_2O, respectively. These water contents are nearly identical to those calculated by Luhr (1992) for Colima lavas using albite-anorthite liquid equilibrium (2.5–4.8 wt.% H_2O). One melt inclusion from orthopyroxene taken from Colima's 1890 lava flow (M82-11 PXMI 1) was significantly drier with only 0.72 ± 0.07 wt.% H_2O, while one hosted in plagioclase from the 1869 eruption (sample 1004-414-PLMI, 1869) contained 0.39 ± 0.03 wt.% H_2O; near the detection limit of the ion probe.

CO_2 concentrations in Popocatépetl melt inclusions range from 102 ± 15 to 1458 ± 219 ppm. Most Popocatépetl melt inclusions (28 out of 38 melt inclusions measured by SIMS) contain 250–750 ppm CO_2; however, melt inclusions from *Atla* are generally higher in CO_2 (466–1458 ppm CO_2 with an average concentration of 953 ppm CO_2) than samples from any other group (Table 3). Melt inclusions from *Amec* and *Tetel* groups are fairly consistent and range between 322–939 (average concentration of 633 ppm CO_2) and 240–866 ppm CO_2 (average concentration of 493 ppm CO_2), respectively. The 2 *Chol* melt inclusions contain CO_2 concentrations of 102 and 380 ppm (average concentration of 241 ppm CO_2).

Water correlates inversely with K_2O (Fig. 5). Because potassium is our best indicator of degree of

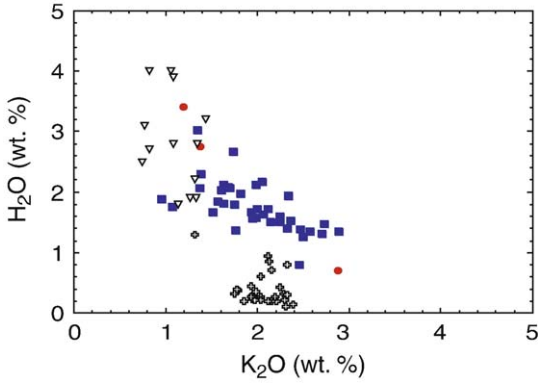

Fig. 5. Plot of H_2O vs. K_2O for Popocatépetl (■) and Colima (●) melt inclusions. Data from Xitle (✜) (Cervantes and Wallace, 2003) and Paricutin melt inclusions (▽)(Luhr, 2001) are included for comparison.

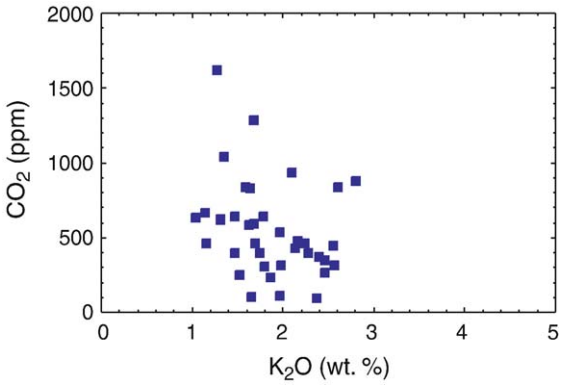

Fig. 6. Plot of K_2O vs. CO_2 for Popocatépetl melt inclusions. Although data are scattered CO_2 generally decreases with increasing K_2O.

differentiation in Popocatépetl and Colima lavas, a steady decrease in H_2O concentration as potassium increases is indicative of degassing as the melt becomes more differentiated. Although CO_2 concentrations show a wide range at a given SiO_2 or K_2O, there is an overall negative correlation with K_2O and positive correlation with H_2O (Fig. 6). Thus, as the melts become more differentiated, both H_2O and CO_2 concentrations decrease. Therefore we suggest these melts reflect vapor-saturated crystallization driven by degassing during ascent, as discussed below.

5. Discussion

5.1. Vapor-saturated crystallization during ascent

There are three possible ways that magmatic H_2O and CO_2 can vary as a function of differentiation, pressure and style of degassing (Fig. 7):

(1) During mixed H_2O–CO_2 vapor-saturated crystallization at constant pressure in a closed system, crystallization will enrich the residual magma in H_2O. As the concentration of water in the melt increases, the proportion (fugacity) of water in the equilibrium vapor phase increases, resulting in a decrease in the proportion of CO_2 in the vapor phase and a decrease in the saturation value of CO_2. Thus progressive crystallization under theses conditions produces an inverse relationship between water and CO_2 in the residual melt (e.g., Newman et al., 1988; Dixon and Stolper, 1995). This behavior is expected for crystallization within stable magma chambers and has been well documented in the Bishop Tuff (Anderson et al., 1989) and in olivine melt inclusions from Nicaragua (Roggensack et al., 1997). Mixed H_2O–CO_2 vapor-saturated crystallization at constant pressure will also produce positive correlations between H_2O and indicators of extent of differentiation such as SiO_2 or K_2O, while producing a negative correlation between CO_2 and SiO_2 or K_2O.

(2) Degassing during ascent without concurrent crystallization will result in rapid CO_2 loss followed by H_2O loss and slower CO_2 loss once H_2O concentrations approach the H_2O solubility limit. The curvature of the degassing trend is a function of the style of degassing (open or closed system behavior) and the initial volatile content (Dixon and Stolper, 1995; Newman and Lowenstern, 2002). Degassing paths for Mono Craters, which represent small batches of magma degassing during ascent to the surface, clearly show this effect (Newman et al., 1988; Anderson et al., 1989). This style of degassing produces no significant trends between indicators of extent of differentiation and volatiles.

(3) If crystallization accompanies degassing during ascent, then H_2O and CO_2 will vary inversely with SiO_2 or K_2O, while simultaneously producing the degassing trend shown in Fig. 7. The overall trends in our data are consistent with this mechanism. This suggests that the magmas are vapor-saturated during crystallization and that degassing and crystallization occur simultaneously during ascent (depressurization).

5.2. Calculated pressures of vapor-saturated crystallization

Dissolved water and carbon dioxide concentrations in glasses can be used to calculate the pressure at which the corresponding melt was last vapor-saturated, and the composition of the co-existing vapor phase at (e.g. Newman et al., 1988; Dixon and Stolper, 1995; Dixon,

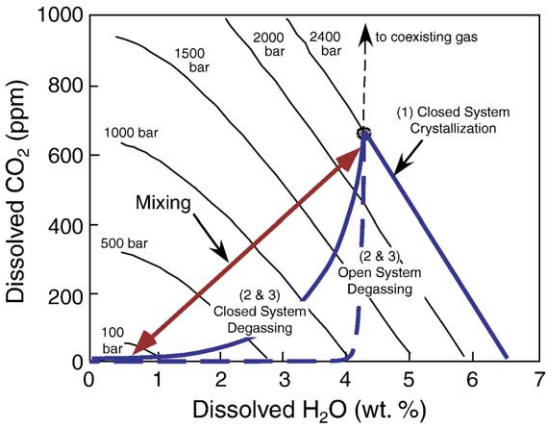

Fig. 7. Behavior of H_2O and CO_2 concentrations as a function of closed system crystallization from a given starting vapor composition, closed system degassing of the same vapor composition and mixing between volatile-rich and degassed end members. Figure modeled after Anderson et al. (1989).

1997; Newman and Lowenstern, 2002). In the case of melt inclusions, these vapor-saturation pressures provide information on the pressures of melt entrapment, hence depths of crystallization. These studies show the importance of using combined H_2O and CO_2 to calculate vapor-saturation pressures.

Popocatépetl melt inclusions contain between 0.80 and 2.5 wt.% H_2O and 100 and 1000 ppm CO_2. Using the rhyolite vapor-saturation model of Newman and Lowenstern (2002) we calculate entrapment pressures for dacitic to rhyolitic melt inclusions between ~280 and ~3000 bars (Table 3). Assuming a crustal density of 2.5 g/cm^3 (appropriate for an overburden of vesiculated block lava, pumice, ash fall and scoria layers), these pressures are equivalent to 1 to 12 km depth. Most of our melt inclusions correspond to entrapment pressures between ~500 and ~2000 bar at 1050 °C (see Straub and Martin-Del Pozzo 2001 for an explanation of temperature used) (Table 3), equivalent to depths of 2 to 8 km. Pressures recorded by Popocatépetl melt inclusions are consistent with the range of pressures for crystallization derived for Popocatépetl, Colima and other Mexican andesites. The upper range of crystallization depths estimated by low Mg# clinopyroxene and plagioclase equilibrium for Popocatépetl lava is 3000–4000 bar (Straub and Martin-Del Pozzo, 2001), while the average estimated depth of magma stagnation at Popocatépetl is between 1 and 4 km (Straub and Martin-Del Pozzo, 2001). At Colima, Moore and Carmichael (1998) estimate P_{H_2O} between 700 and 2500 bar. Carmichael (2002) estimates crystallization pressures between 2000 and 4000 bar for intermediate lava from West Mexico (Fig. 8). At Zitacuaro and Valle de Bravo volcanoes, Blatter and Carmichael (1998, 2001) estimate crystallization pressures between 300 and 3000 bars. These pressure ranges agree well with the estimated maximum and average pressures recorded by our melt inclusions.

In the absence of CO_2 data (e.g. our Colima samples), water concentrations can be compared to water solubility models to obtain a minimum estimate of vapor-saturation pressure. Work by Moore et al. (1995, 1998) models the solubility of water in silicate liquids as a function of melt composition, temperature and pressure. Calculating pressure for a CO_2 free system, water-rich melt inclusions from Volcán de Colima (3.0–3.4 wt.% H_2O) would be saturated with pure H_2O vapor at ~750 to 900 bar or 3 to 3.6 km (assuming 950 °C, see Moore et al., 1995, 1998; Blatter and Carmichael, 2001) (Fig. 8). These pressures compare well to those calculated for Colima andesite (P_{H_2O} = 500–2000 bar) by

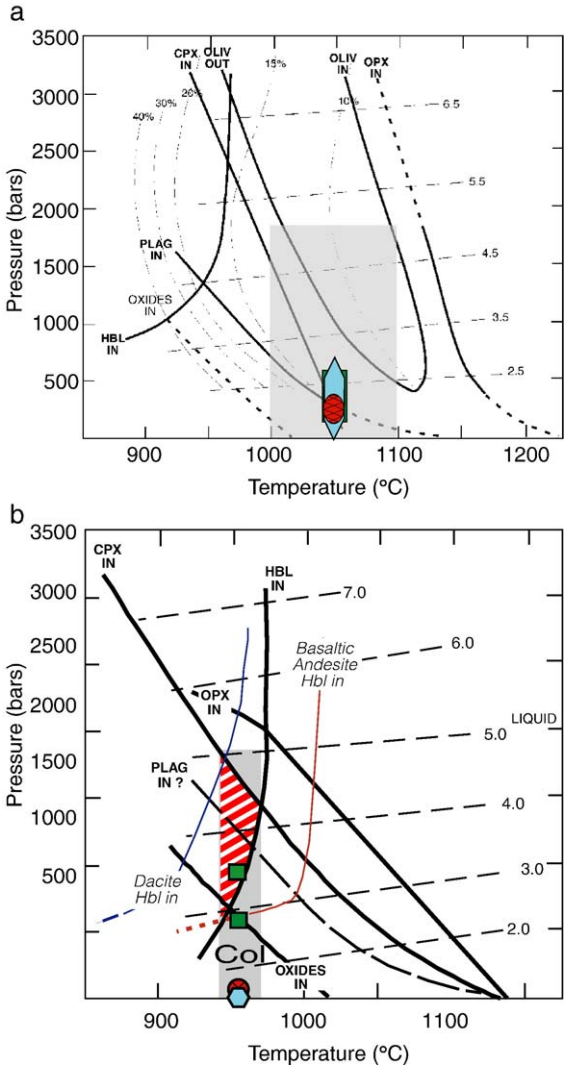

Fig. 8. Phase stability diagram for Popocatepetl (a) and for Colima (b) as compared to crystallization depth based on melt inclusion water content (cyan hexagons are plagioclase hosted inclusions, red hatched circles represent opx, and green squares are cpx hosted inclusions). Shaded areas represent possible isothermal decompression paths for Colima and Popocatépetl lava based on magmatic temperatures calculated by Luhr and Carmichael (1990) and by Straub and Martin-del Pozzo (2001), respectively. Thick dashed lines represent water saturation isopleths from Moore and Carmichael (1998). Thick solid lines are phase stability boundaries. Thin dashed line represents degree of crystallintiy. Diagram was modified from Blatter and Carmichael (2001) and Moore and Carmichael (1998). (For interpretation of the references to colour in this figure legend, the reader is referred to the web version of this article.)

Moore et al. (1995, 1998). Our water-poor melt inclusions correspond to minimum entrapment pressures of P_{H_2O} = 16 to 53 bar or less than 200 m depth. Higher pressures would be required if the vapor contained significant amounts of CO_2 (Dixon and Stolper, 1995; Blank et al., 1993).

5.3. Degassing models

In order to investigate pre-eruptive volatile content and degassing history we have taken water and CO_2 data for Popocatépetl and calculated possible degassing paths using *VolatileCalc* (Newman and Lowenstern, 2002). VolatileCalc calculates progressive equilibrium H_2O and CO_2 concentrations in the melt during depressurization (degassing paths) based on input values of temperature, pressure, and H_2O and CO_2 concentrations in the melt. For closed system degassing, the user must also input the weight percent exsolved volatiles, which may be added back to a given melt inclusion composition to estimate minimum starting compositions. Equilibrium vapor compositions can also be calculated by VolatileCalc for a melt with known dissolved water and CO_2 concentrations. We have used this model and investigated various postulated starting compositions ranging from 1.5 to 6.0 wt.% H_2O and 1500 ppm to 1 wt.% CO_2. We have also investigated a starting volatile content equal to our most volatile-rich inclusions. In all cases open-system degassing paths failed to reproduce the trends in H_2O and CO_2 at Popocatépetl. However, closed-system degassing models generate degassing paths that bracket our data quite well (Fig. 9a). The water-rich, lower CO_2 melt inclusions require the melt to be in equilibrium with 17 wt.% exsolved volatiles in order to minimize the misfit between the model and our data. For the CO_2-rich melt inclusion, only 3 wt.% exsolved volatiles are required. Though VolatileCalc is not useful for unique determination of starting concentrations (numerous starting composition will produce appropriate degassing paths), the amount of exsolved volatiles needs to be kept within ± 2 wt.% of the above values to produce suitable degassing paths.

We can evaluate if the model results are physically reasonable by estimating the initial volatile compositions. We do this by adding the amount of exsolved vapor to the amount dissolved in the melt inclusion (Newman and Lowenstern, 2002). By adding 17 wt.% exsolved volatiles (30 mol% H_2O and 70 mol% CO_2) to the melt inclusion with the highest water content (3.02 wt.% H_2O, 1045 ppm CO_2), we find that a parental magma should contain a minimum of 8 wt.% H_2O and 14 wt.% CO_2. For the CO_2-rich, H_2O-poor melt inclusion (the most volatile-rich melt inclusion on the 3 wt.% exsolved vapor (10 mol% H_2O and 90 mol% CO_2) path in Fig. 9a), we calculate a parent with ~1.7 wt.% H_2O and 3.0 wt.% CO_2. These values could be substantially higher if we consider the addition of a trapped vapor bubble(s) within some of our melt inclusions (Danyushevsky et al., 2002). While the water

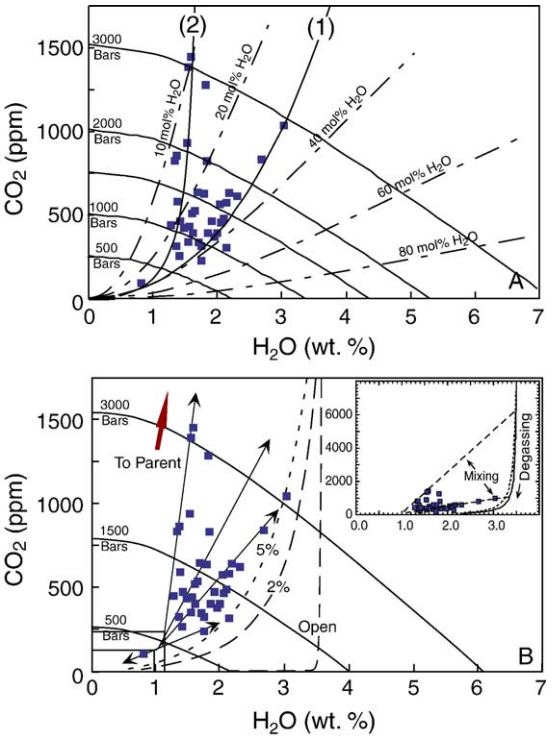

Fig. 9. Plot of H_2O vs. CO_2 for Popocatepetl melt inclusions. Isobars, isopleths and degassing paths were calculated using VolatileCalc (Newman and Lowenstern, 2002) for rhyolite liquids at 1050 °C. (A) Closed system degassing paths for two different hypothetical liquids that bound the melt inclusion data are shown. Starting compositions are (1) 5 wt.% H_2O, 4000 ppm CO_2 in equilibrium with 17% and (2) 1.75 wt.% H_2O, 4000 ppm CO_2 in equilibrium with 3% exsolved vapor. (B) Mixing model (solid lines delineate 4 separate mixtures although other paths are equally plausible) with closed system degassing paths calculated from a single parental magma containing 3.5 wt.% H_2O and 1.0 wt.% CO_2. Dashed lines represent degassing paths for open system behavior and closed system behavior with 2% and 5% exsolved volatiles in equilibrium with the melt. Boxes in lower left corner is suggested pressure range for degassed magma.

contents are not unreasonable for primitive Mexican magmas (Carmichael, 2002; Martin Del Pozzo et al., 2003 and references therein) the calculated CO_2 content (14 wt.%) seems unreasonably high, although CO_2 contents of Mexican magmas have not been previously reported (Blank et al., 1993; King and Holloway, 2002). Moreover, the solution is non-unique; two sources with different water contents, but similar CO_2 contents, are required to explain all the data. This seems unreasonable, and suggests that the observed trends in volatile concentration are not controlled simply by closed system degassing during ascent.

Alternatively, we can consider a series of mixing lines that trend through our data to a parental magma that is rising and degassing (Fig. 9b). Doing so allows us

to use a single parental magma composition to explain all the data. Moreover, mixing makes closed system degassing with far less exsolved volatiles possible and also allows the possibility of open system degassing. To illustrate, if we draw a series of mixing lines that encompass most of our data and use an open system degassing model starting with 3.5 wt.% water and 6000 ppm CO_2, mixing between mafic un-degassed and more evolved, degassed magma explains this data well (Fig. 9b). Alternatively, we can also consider a parental magma compositions with more dissolved water (e.g. at 6 wt.% H_2O (Carmichael, 2002 and references therein) CO_2 concentration would have to be 1.2 ± 0.3 wt.% to equally explain the data. At 4–5 wt.% H_2O (see discussions by Luhr and Carmichael, 1990; Luhr, 1992, 2001; Moore and Carmichael, 1998; Blatter and Carmichael, 2001) the magma would contain roughly between 7000 and 9000 ppm CO_2. While there is room for variation in H_2O starting compositions, we cannot increase this concentration much beyond 6 wt.% without making CO_2 values unreasonably high.

Our allowable mixing lines converge between 0.95 and 1.25 wt.% H_2O and 115 and 225 ppm CO_2. Magma with these concentrations would be saturated between 280 and 720 bars (1.1 and 2.9 km) at temperatures ranging from 950 to 1170 °C (Straub and Martin-Del Pozzo, 2001; Martin Del Pozzo et al., 2003). We suggest that these depths (albeit minimal estimates, see Danyushevsky et al., 2002) may represent a zone of mixing between an undegassed, mafic end member and a degassed, evolved end member.

5.4. Pressure of crystallization and major element trends

Much of the compositional variation of lavas at the different volcanic centers is produced by crystallization within the upper few kilometers of crust (Hasenaka and Carmichael, 1987). Similarly, vapor-saturated crystallization during ascent can be used to explain melt inclusion composition. When plotted on an alkali–iron–magnesium (AFM) diagram along with volcanics from other parts of México, some Mexican volcanics follow the "classical" calc-alkali trend, while many of our melt inclusions follow a "tholeiitic-type" trend (Fig. 10). While we do not suggest that our melt inclusions have been produced by a tholeiitic parent, we recognize other ways to produce such a trend. One simple way is to fix the oxygen fugacity to the quartz–fayalite–magnetite buffer. However, Popocatépetl and V. Colima's magmas develop under oxidizing conditions (NNO − NNO + 1) (Blatter and Carmichael, 2001; Straub and Martin-Del Pozzo, 2001; Luhr and Carmichael, 1990). Another possibility is to fractionally crystallize olivine and py-

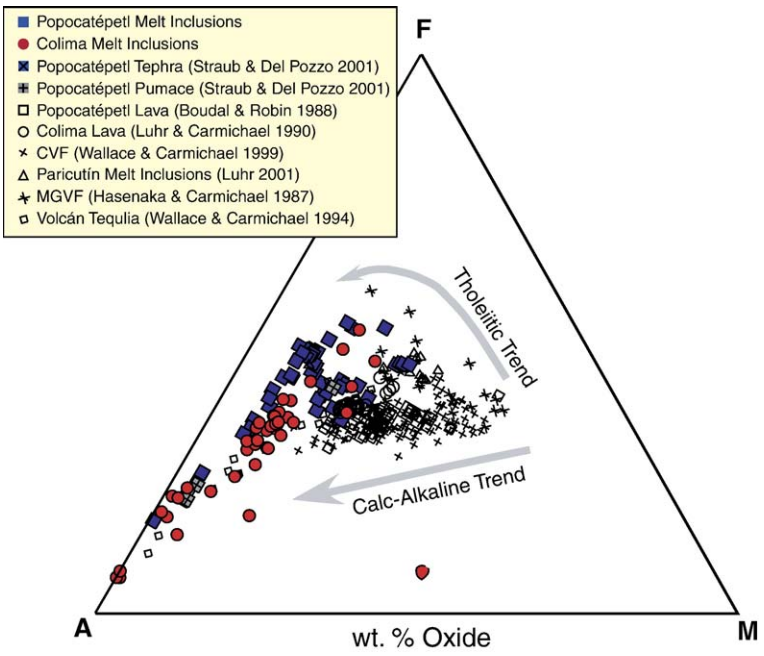

Fig. 10. AFM Diagram for Popocatépetl and Colima melt inclusions and their respective host lava and tephra. Also plotted are primitive and evolved magmas from the Trans-Mexican Volcanic Belt. Tholeiitic and calc-alkaline trends are shown and are representative of crystallization in dry and wet conditions, respectively.

roxene at low pressure (Grove and Kinzler, 1986). Doing so will push the liquids away from MgO towards FeO and alkali apices in the AFM diagram. Which of the two apices the liquids move to depends on the H_2O content of the magma. Gaetani et al. (1993), Sisson and Grove (1993), and Blatter and Carmichael (1998, 2001) show that at high P_{H_2O} (under vapor saturated conditions) plagioclase will not crystallize. This produces a calc-alkaline trend (e.g., liquid compositions will move towards Na_2O+K_2O). However if P_{H_2O} decreases due to degassing (and the magmas remain vapor-saturated but at lower pressure), plagioclase will crystallize and the trend will be pushed towards the FeO apex. As magnetite (ilmenite) joins the crystallizing assemblage, the liquids will again move towards Na_2O+K_2O even at high oxygen fugacity (Sisson and Grove, 1993). Therefore, vapor-saturated crystallization during degassing is capable of producing the observed tholiitic trend.

We can also test our model of vapor-saturated crystallization during ascent by comparison to results of vapor-saturated crystallization experiments. Fig. 11 plots our data on an olivine–augite–quartz diagram (modified from Grove et al., 1982; Grove and Kinzler, 1986; Sisson and Grove, 1993), illustrating the effect of increasing water pressure on cotectics in this system. While we realize their experiments start with high-alumina basalt typical of the Cascade arc and not of Mexico, we can still draw several important conclusions from such a comparison. For Mexican lavas, early crystallization of olivine is evident in the most mafic samples and continues until the liquid composition reaches an implied cotectic between 1 and 2 kbar P_{H_2O}. From here the liquid line of descent shifts towards the 1 kbar cotectic. The remainder of the compositions, including our melt inclusions, lie between the 1 kbar to 1 atm (dry) cotectics. This is consistent with vapor saturated crystallization during ascent from pressures of ~2 kbar to near surface conditions. The variability in water content measured in plagioclase and orthopyroxene melt inclusions (0.3–2.9 and 0.7–3.0 wt.% H_2O, respectively) are also consistent with crystallization trends predicted by ol-aug-qz and ol-plag-qz diagrams (Fig. 12). Moreover, the derived pressures are also consistent with the pressure derived for the most volatile rich inclusion from Colima (in cpx) which would have been entrapped at ≤2 to just under 1.8 kb. Therefore, while this result obtained from the ol-aug-qz diagram does not preclude mixing, because any mixture will also fall on the differentiation line, it does suggest that vapor-saturated crystallization at decreasing water pressure has a strong influence on the evolution of these magmas.

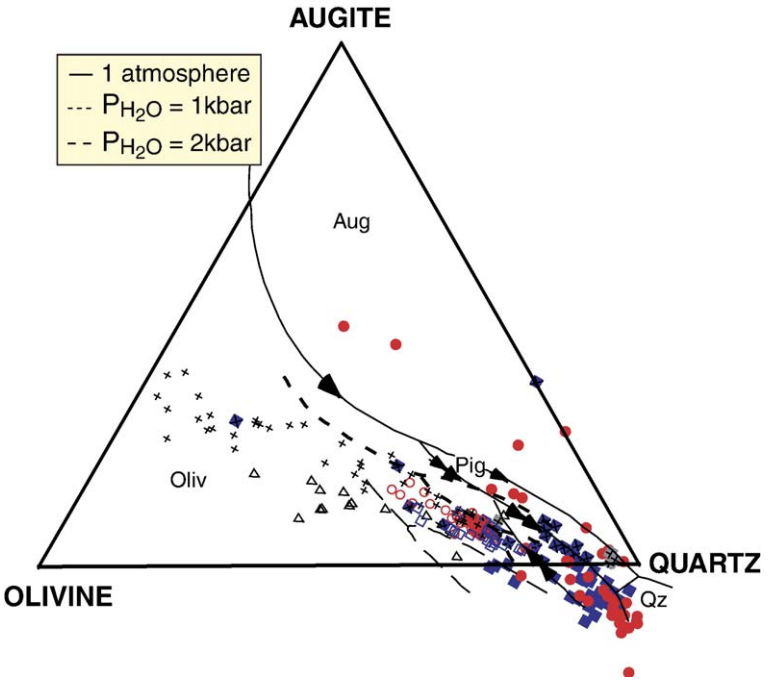

Fig. 11. Melt inclusion composition for both Colima and Popocatépetl compared to other Mexican volcanics including Colima and Popocatépetl lavas. Compositions for melt inclusions fall on or between 1 kbar and 1 atm (dry) cotectics. Diagram illustrates early fractionation of olivine followed by crystallization of cpx, pig then opx between 1 and 2 kbar P_{H_2O} (figure modified from Grove et al., 1997; Sisson and Grove, 1993; Grove and Kinzler, 1986). Symbols are the same as Fig. 10.

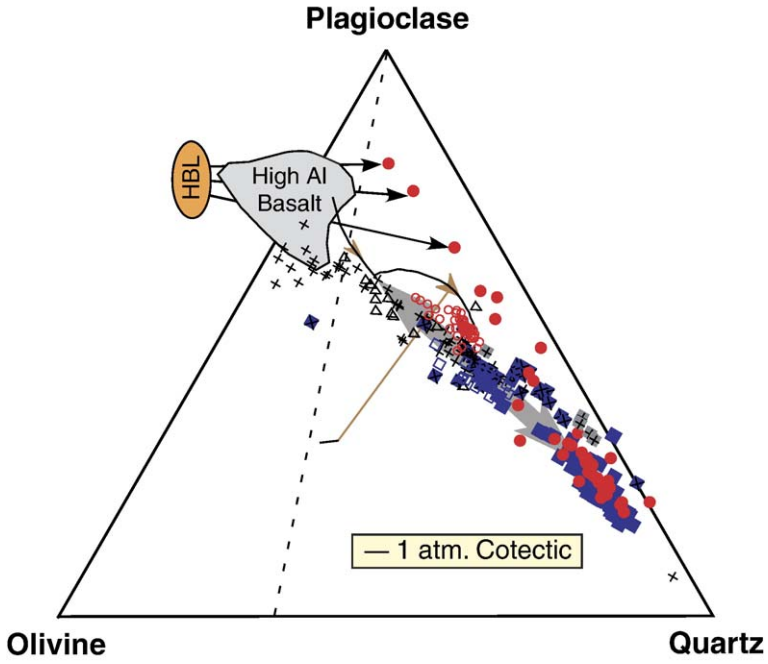

Fig. 12. Olivine–plagioclase–quartz pseudo ternary diagram for Colima and Popocatepetl melt inclusions and other Mexican volcanics. Diagram shows fractionation of hornblende from HAB type source (Grove et al., 1982; Johnson et al., 1994; Grove et al., 1997) to be prevalent in some samples. Near cotetic crystallization (1 atm) and mixing (gray shaded arrow) are likely (figure modeled after Grove et al., 1997; Sisson and Grove, 1993; Grove et al., 1982). Symbols are the same as Fig. 10.

5.5. Implications for magmatic plumbing systems

Classical views of magmatic systems often include the concept of a large, mid to shallow crustal magma chamber. Such chambers are generally considered to be at fixed depth. Recent research on melt evolution has suggested that magma crystallization occurs in crystallization fronts in smaller sills placed at different depths (Marsh, 1989, 2002). Stagnation of magma at these fronts can lead to highly evolved compositions. At ~50% or more crystallization, the residual crystal "mush" becomes quasi-solid; evolved compositions are stuck in the interstices and may not be expressed at the surface (Marsh, 1994, 1998). The implication is that rhyolites sampled by melt inclusions represent interstitial liquid within a crystal mush.

However, the volatile concentrations in Popocatépetl and Colima melt inclusions do not indicate stagnation at any particular depth (see Figs. 9–12). Moreover there is no correlation between pressure and indicators of crystallization such as SiO_2 and K_2O (Fig. 13) indicating that crystallization also did not occur at any given depth. We would expect a single vapor saturation pressure for a magma chamber and a systematic series of pressures if vapor-

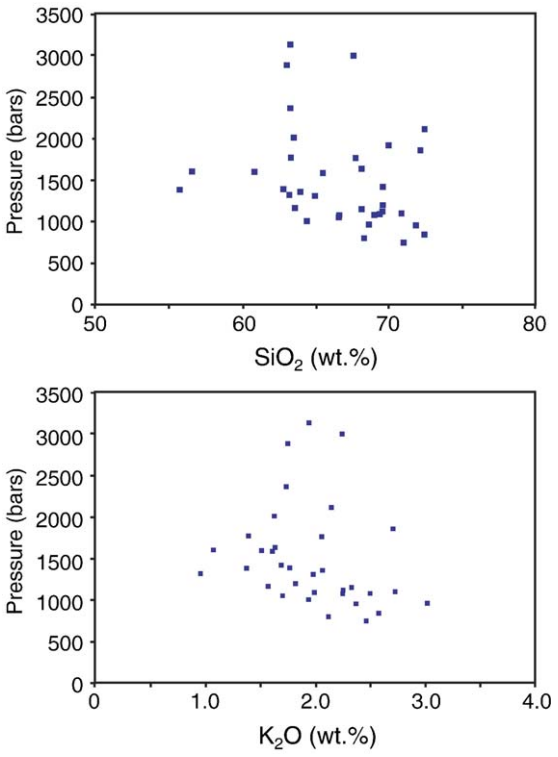

Fig. 13. K_2O and SiO_2 melt inclusion compositions for Popocatépetl plotted against depth.

saturated crystallization occurred in a series of perched sills. Research has already shown that the parent magma for both Popocatépetl and Colima is a mantle-derived hydrous basaltic parent (Straub and Martin-Del Pozzo, 2001; Carmichael, 2002). The presence of only small amounts of andesitic (~55% SiO_2) degassed melt inclusions while more evolved melts reside above and below and at the same depth, suggests that andesites may be uncommon at depth. The fact that no rhyolites are expressed on the surface does not necessarily indicate that they are "stuck," but instead may suggest that they slow down during ascent due to increases in viscosity from degassing and subsequent crystallization (Dixon et al., 1991; Lange, 1994; Wallace and Anderson, 1998). Later these melts may be remobilized by fresh batches of hotter, more volatile-rich magma (Marsh, 1998). Thus, either the parent melt bypasses the evolved magma and is erupted elsewhere, or, more likely, is mixed with an evolved magma en-route to the surface. The lack of any systematic pressure-composition relationship seems to indicate that there is no single location or systematic series of locations where this is occurring. We envision a dynamic process with vapor-saturated crystallization during ascent combined with mixing of a relatively degassed evolved melt and a less degassed, primitive melt in the upper few kilometers of crust. Stagnation at any particular depth did not occur, and a large stratified magma chamber or series of stratified sills is not required.

5.6. Implications for volcanic deformation

As a concluding note, it has recently been pointed out that GPS data indicate little or no surface deformation during the recent eruptions at Popocateptl (Cabral and Dixon, 2002; www.geodesy.miami.edu/volcano.html). This "eruption without deformation" has also been observed at Mt. St. Helens (Dzurisin et al., 2005). If small volumes of magma crystallize under vapor-saturated conditions during ascent in conduits with no large magma chamber during effusive periods, this could provide an explanation for the lack of deformation. For very large eruptions (e.g., Mt. St. Helens 1980, Pinatubo 1991, etc.) large batches of magma may form an upper crustal magma chamber that should cause extensive surface deformation. But at Popocatépetl no significant surface swelling was present during dome growth of the middle 1990s (Cabral and Dixon, 2002). Similarly, at Colima, little to no tilt was recorded during its dome building period in the 1980s (Murray, 1993). Moreover, Colima has been subsiding and not inflating as would be expected from a swelling magma chamber during the eruptive period of 1982–1999 (Murray and Wooller, 2002). Events at Colima during the latter part of this period recorded deformation only at or near the summit suggesting a localized or small injection of magma consistent with our model (Ramírez-Ruiz et al., 2002). Finally seismic evidence from the 1991 eruption of Colima shows a seismic swarm at depths between 1 and 4 km (Núnez-Cornú et al., 1994). We suggest that these seismic swarms could be produced by ascent, crystallization and exsolution of volatiles from a number of small magma bodies.

6. Conclusions

Melt inclusions from Popocatépetl and Volcán de Colima are highly evolved and have been produced from vapor-saturated crystallization in combination with mixing in small batches during ascent. Water concentrations in melt inclusions from Popocatépetl and Colima are similar and are consistent with entrapment at pressures of 3 kbar or less. Major element variation is also consistent with vapor-saturated crystallization at pressures below 2 kbar. Our results show that the dacitic to rhyolitic melt sampled by these melt inclusions were entrapped continually throughout the ascent process. We suggest that vapor-saturated crystallization during ascent in a series of interconnected conduits in which mixing is allowed is more plausible for the Popocatépet and Colima volcanic systems. We thus find no compelling evidence for a large magma chamber at either Popocatépetl or Colima for the periods of time in which these samples were erupted.

Acknowledgments

The authors would like to thank James F. Luhr for providing the Colima samples as well as Hugo Delgado for assistance in providing Popocatépetl samples. We would also like to thank Eric Hauri (Department of Terrestrial Magmatism of the Carnegie Institute of Washington) and Richard Hervig (Arizona State University) for their assistance with the ion microprobe. We are grateful to Tom Beasley and FCAEM (Florida International University) for the many hours of assistance with the electron microprobe. The manuscript was greatly improved by the thoughtful reviews from Dawnika Blatter, Susanne Straub and an anonymous reviewer. Analysis of Popocatépetl samples was supported by NSF Grant EAR9527273.

Appendix A. Supplementary Data

Supplementary data associated with this article can be found, in the online version, at doi:10.1016/j.jvolgeores.2005.06.010.

References

Allan, J.F., Carmichael, I.S.E., 1984. Lamprophyric lavas in the Colima Graben, SW Mexico. Contributions to Mineralogy and Petrology 88 (3), 203–216.

Anderson, A.T., Newman, S., Williams, S.N., Druitt, T.H., Skirius, C.M., Stolper, E., 1989. H_2O, CO_2, Cl and gas in plinian and ash-flow Bishop rhyolite. Geology 17, 221–225.

Blank, J.G., Stolper, E.M., Carroll, M.R., 1993. Solubilities of carbon dioxide and water in rhyolitic melt at 850 C and 750 bars. Earth and Planetary Science Letters 119, 27–36.

Blatter, D.L., Carmichael, I.S.E., 1998. Plagioclase-free andesites from Zitácuaro (Michoacán), Mexico: petrology and experimental constraints. Contributions to Mineralogy and Petrology 132, 121–138.

Blatter, D.L., Carmichael, I.S.E., 2001. Hydrous phase equilibria of Mexican high-silica andesite: a candidate for a mantle origin? Geochimica et Cosmochimica Acta 65 (21), 4043–4065.

Boudal, C., Robin, C., 1988. Relations entre dynamismes éruptifs et réalimentations magmatiques d'origine profonde au Popocatépetl. Canadian Journal of Earth Science 25, 955–971.

Cabral, E., Dixon, T., 2002. Geodesy website, University of Miami (RSMAS). www.geodesy.miami.edu/volcano.html.

Carmichael, I.S.E., 2002. The andesite aqueduct: perspectives on the evolution of intermediate magmatism in west-central (105–95° W) México. Contributions to Mineralogy and Petrology 143, 641–663.

Cawthorn, R.G., Curran, E.B., Arculus, R.J., 1973. A petrogenetic model for the origin of the calc-alkaline suite of Grenada, Lesser Antilles. Journal of Petrology 14 (2), 327–337.

Cervantes, P., Wallace, P., 2003. Magma degassing and basaltic eruption styles: a case study of ~2000 year B.P. Xitle volcano in central Mexico. Journal of Volcanology and Geothermal Research 120 (3–4), 249–270.

Chesley, J., Ruiz, J., Righter, K., Ferrari, L., Gomez-Tuena, A., 2002. Source contamination versus assimilation: an example from the Trans-Mexican Volcanic Arc. Earth and Planetary Science Letters 195, 211–221.

Danyushevsky, L.V., McNeill, A.W., Sobolev, A.V., 2002. Experimental and petrological studies of melt inclusions in phenocrysts from mantle-derived magmas: an overview of techniques, advantages and complications. Chemical Geology 183, 5–24.

De La Cruz-Reyna, S., 1993. Random patterns of occurrence of explosive eruptions at Colima Volcano, Mexico. Journal of Volcanology and Geothermal Research 55 (1–2), 51–68.

Devine, J.D., Rutherford, M.J., Gardner, J.E., Brack, H.P., Layne, G.D., 1995. Comparison of microanalytical methods for estimating H_2O contents of silicic volcanic glasses. American Mineralogist 80 (3–4), 319–328.

Dixon, J.E., 1997. Degassing of alkalic basalts. American Mineralogist 82, 368–378.

Dixon, J.E., Stolper, E.M., 1995. An experimental study of water and carbon dioxide solubilities in mid-ocean ridge basaltic liquids: Part II. Application to degassing. Journal of Petrology 36 (6), 1633–1646.

Dixon, J.E., Clague, D.A., 2001. Volatiles from Loihi Seamount, Hawaii: evidence for a relatively dry plume component. Journal of Petrology 42 (3), 627–654.

Dixon, J.E., Clague, D.A., Stolper, E.M., 1991. Degassing history of water, sulfur, and carbon in submarine lavas from Kilauea Volcano, Hawaii. Journal of Geology 99, 371–394.

Dixon, J.E., Stolper, E.M., Holloway, J.R., 1995. An experimental study of water and carbon dioxide solubilities in mid-ocean ridge basaltic liquids: Part I. Calibration and solubility models. Journal of Petrology 36 (6), 1607–1631.

Dunbar, N.W., Hervig, R.L., 1992. Volatile and trace element composition of melt inclusions from the Lower Bandelier Tuff: implications for magma chamber process and eruptive style. Journal of Geophysical Research 97 (B11), 15151–15170.

Dunbar, N.W., Hervig, R.L., Kyle, P.R., 1989. Determination of pre-eruptive H_2O, F and Cl contents of silicic magmas using melt inclusions: examples from Taupo volcanic center, New Zealand. Bulletin of Volcanology 51, 177–184.

Dzurisin, D., Vallance, J.W., Gerlach, T.M., Moran, S.C., Malone, S.D., 2005. Mount St. Helens reawakens. EOS Transactions, American Geophysical Union 86 (3), 25–29.

Gaetani, G.A., Grove, T.L., Bryan, W.B., 1993. The influence of water on the petrogenesis of subduction-related rocks. Nature 365, 332–334.

Gioncada, A., Clocchiatti, R., Sbrana, A., Bottazzi, P., Massare, D., Ottolini, L., 1998. A study of melt inclusions at Vulcano (Aeolian Islands, Italy): insights on the primitive magmas and on the volcanic feeding system. Bulletin of Volcanology 60, 286–306.

Grove, T.L., Kinzler, R.J., 1986. Petrogenesis of andesites. Annual Review of Earth and Planetary Science 14, 417–454.

Grove, T.L., Gerlach, D.C., Sando, T.W., 1982. Origin of calc-alkaline series lavas at Medicine Lake volcano by fractionation, assimilation and mixing. Contributions to Mineralogy and Petrology 80, 160–182.

Grove, T.L., Donnelly-Nolan, J.M., Housh, T., 1997. Magmatic processes that generated, the rhyolite of Glass mountain, Medicine Lake volcano, N. California. Contributions to Mineralogy and Petrology 127, 205–223.

Hasenaka, T., Carmichael, I.S.E., 1987. The cinder cones of Michoacán-Guanajuato, central Mexico: petrology and chemistry. Journal of Petrology 28, 241–269.

Hauri, E., King, P.L., Mandeville, C.W., Newman, S., Wang, J., Dixon, J.E., 2002. SIMS analysis of volatiles in volcanic glasses: 1. Calibration, matrix effects and comparisons with FTIR. Chemical Geology 183, 99–114.

Hawkesworth, C.J., Blake, S., Evans, P., Hughes, R., MacDonald, R., Thomas, L.E., Turner, S.P., Zellmer, G., 2000. Time scales of crystal fractionation in magma chambers; integrating physical, isotopic and geochemical perspectives. Journal of Petrology 41 (7), 991–1006.

Hervig, R.L., Dunbar, N.W., 1992. Cause of chemical zoning in the Bishop (California) and Bandelier (New México) magma chambers. Earth and Planetary Science Letters 111, 97–108.

Hervig, R.L., Dunbar, N., Westrich, H.R., Kyle, P.R., 1989. Pre-eruptive water content of rhyolitic magmas as determined by ion microprobe analyses of melt inclusions in phenocrysts. Journal of Volcanology and Geothermal Research 36, 293–302.

Ihinger, P.D., Hervig, R.L., McMillian, P.F., 1994. Analytical methods for volatiles in glasses. In: Carrol, M.R., Holloway, J.R.

(Eds.), Volatiles in Magmas. Reviews in Mineralogy, vol. 30, pp. 67–112.
Johnson, M.C., Anderson, A.T., Rutherford, M.J., 1994. Pre-eruptive volatile contents of magmas. In: Carrol, M.R., Holloway, J.R. (Eds.), Volatiles in Magma. Reviews in Mineralogy, vol. 30, pp. 281–330.
Kamenetsky, V.S., Crawford, A.J., Eggins, S., Mühe, R., 1997. Phenocryst and melt inclusion chemistry of near-axis seamounts, Valu Fa Ridge, Lau Basin: insight into mantle wedge melting and the addition of subduction components. Earth and Planetary Science Letters 151, 205–223.
King, P.L., Holloway, J.R., 2002. CO_2 solubility and speciation in intermediate (andesitic) melts: the role of H_2O and composition. Geochimica et Cosmochimica Acta 66 (9), 1627–1640.
Lange, R.A., 1994. The effect of H_2O, CO_2 and F on the density and viscosity of solicate melts. In: Carrol, M.R., Holloway, J.R. (Eds.), Volatiles in Magma. Reviews in Mineralogy, vol. 30, pp. 331–369.
Lee, J., Stern, R.J., 1998. Glass inclusions in Mariana Arc phenocrysts: a new perspective on magmatic evolution in typical intra-oceanic are. Journal of Geology 106, 19–33.
Luhr, J.F., 1992. Slab-derived fluids and partial melting in subduction zones: insights from two contrasting Mexican volcanoes (Colima and Ceborucco). Journal of Volcanology and Geothermal Research 54, 1–18.
Luhr, J.F., 1993. Petrology and geochemistry of stage: I. Andesites and dacites from the caldera wall of Volcán Colima, Mexico. Geofisica Internacional 32 (4), 591–603.
Luhr, J.F., 2001. Glass inclusions and melt volatile contents at Paricutín volcano, México. Contributions to Mineralogy and Petrology 142, 261–283.
Luhr, J.F., Carmichael, I.S.E., 1980. The Colima volcanic complex, México. Contributions to Mineralogy and Petrology 71, 343–372.
Luhr, J.F., Carmichael, I.S.E., 1981. The Colima volcanic complex, Mexico: Part II. Late-Quaternary cinder cones. Contributions to Mineralogy and Petrology 76, 127–147.
Luhr, J.F., Carmichael, I.S.E., 1982. The Colima volcanic complex, Mexico: III. Ash- and scoria-fall deposits from the upper slopes of Volcán Colima. Contributions to Mineralogy and Petrology 80, 262–275.
Luhr, J.F., Kyser, T.K., 1989. Primary igneous analcime: the Colima minettes. American Mineralogist 74, 216–223.
Luhr, J.F., Carmichael, I.S.E., 1990. Petrological monitoring of cyclical eruptive activity at Volcán Colima, México. Journal of Volcanology and Geothermal Research 42, 235–260.
Macías, J.L., Capaccioni, B., Conticelli, S., Giannini, L., Martini, M., Rodríguez, S., 1993. Volatile elements in alkaline and calc-alkaline rocks from the Colima graben, México: constraints on their genesis and evolution. Geofisica Internacional 32 (4), 575–589.
Mandeville, C.W., Carey, S.N., Sigurdsson, H., 1996. Magma mixing, fractional crystallization, and volatile degassing during the 1883 eruption of Krakatau Volcano, Indonesia. Journal of Volcanology and Geothermal Research 74, 243–274.
Mandeville, C.W., Timbal, A., Faure, K., Webster, J.D., Rutherford, M.J., Taylor, B.E., 2002. Determination of molar absorptivities for infrared absorption bands of H_2O in andesitic glasses. American Mineralogist 87 (7), 813–821.
Marsh, B.D., 1989. Magma chambers. Annual Review of Earth and Planetary Science Letters 17, 439–474.
Marsh, B.D., 1994. Hallimond lecture; solidification fronts and magmatic evolution. Magmatic Processes; Do the Answers Lie in the Rocks? Mineralogical Society Bulletin, vol. 105, pp. 16–17.
Marsh, B.D., 1998. On the interpretation of crystal size distributions in magmatic systems. Journal of Petrology 39 (4), 553–599.
Marsh, B.D., 2002. On bimodal differentiation by solidification front instability in basaltic magmas: Part 1. Basic mechanics. Geochemica et Cosmochemica Acta 66 (12), 2211–2229.
Martin-Del Pozzo, A.L., Cifuentes-Nava, G., Cabral-Cano, E., Sánchez-Rubio, G., Reyes, M., Martínez-Bringas, A., Garcia, E., Arango-Galvan, C., 2002. Volcanomagnetic signals during the recent Popocatépetl (México) eruptions and their relation to eruptive activity. Journal of Volcanology and Geothermal Research 113, 415–428.
Martin Del Pozzo, A.L., Cifuentes, G., Cabral-Cano, E., Bonifaz, R., Correa, F., Mendiola, I.F., 2003. Timing magma ascent at Popocatepetl Volcano, Mexico, 2000–2001. Journal of Volcanology and Geothermal Research 125, 107–120.
Morgan, G.B., London, D., 1996. Optimizing the electron microprobe analysis of hydrous alkali aluminosilicate glasses. American Mineralogist 81, 1176–1185.
Moore, G., Carmichael, I.S.E., 1998. The hydrous phase equilibria (to 3 kbar) of an andesite and basaltic andesite from western México: constraints on water content and conditions for phenocryst growth. Contributions to Mineralogy and Petrology 130, 304–319.
Moore, G., Vennemann, T., Carmichael, I.S.E., 1995. Solubility of water in magmas up to 2 kbar. Geology 23, 1099–1102.
Moore, G., Vennemann, T., Carmichael, I.S.E., 1998. An empirical model for the solubility of H_2O in magmas to 3 kilobars. American Mineralogist 83, 36–42.
Murray, J.B., 1993. Ground deformation at Colima Volcano, Mexico, 1982 to 1991. Geofisica Internacional 32 (4), 659–669.
Murray, J.B., Wooller, L.K., 2002. Persistent summit subsidence at Volcán de Colima, México, 1982–1999: strong evidence against Mogi deflation. Journal of Volcanology and Geothermal Research 117 (1–2), 69–78.
Newman, S., Lowenstern, J.B., 2002. VolatileCalc: a silicate melt–H_2O–CO_2 solution model written in Visual Basic for excel. Computers and Geosciences 28, 597–604.
Newman, S., Epstein, S., Stolper, E., 1988. Water, carbon dioxide, and hydrogen isotopes in glasses from the ca. 1340 A. D. eruption of the mono craters, CA: constraints on degassing phenomena and initial volatile content. Journal of Volcanology and Geothermal Research 35, 75–96.
Nielsen, C.H., Sigurdsson, H., 1981. Quantitative methods for electron microprobe analysis of sodium in natural glasses. American Mineralogist 66, 547–552.
Nielsen, R.L., Crum, J., Bourgeois, R., Hascall, K., Forsythe, L.M., Fisk, M.R., Christie, D.M., 1995. Melt inclusions in high An plagioclase from the Gorda Ridge: an example of the local diversity of MORB parent magmas. Contributions to Mineralogy and Petrology 122, 34–50.
Nielsen, R.L., Michael, P.J., Sours-Page, R., 1998. Chemical and physical indicator of compromised melt inclusions. Geochimica et Cosmochimica Acta 62, 831–839.
Núñez-Cornú, F., Nava, F.A., De la Cruz-Reyna, S., Jiménez, Z., Valencia, C., García-Arthur, R., 1994. Seismic activity related to the 1991 eruption of Colima Volcano, México. Bulletin of Volcanology 56, 228–237.
Pichavant, M., Martel, C., Bourdier, J.-L., Scaillet, B., 2002. Physical conditions, structure, and dynamics of a zoned magma chamber: Mount Pelée (Martinique, Lesser Antilles Arc). Journal of Geophysical Research 107 (B5). doi:10.1029/2001JB000315.

Ramírez-Ruiz, J.J., Breton-González, M., Santiago-Jiménez, H., Alatorre-Chávez, E., 2002. EDM deformation monitoring of the 1997–2000 activity at Volcán de Colima. Journal of Volcanology and Geothermal Research 117 (1–2), 61–67.

Righter, K., Carmichael, I.S.E., 1996. Phase equilibria of phlogopite lamprophyres from western México: biotite-liquid equilibria and P–T estimates for biotite bearing igneous rocks. Contributions to Mineralogy and Petrology 123, 1–21.

Robin, C., 1984. Le Volcán Popocatépetl (Mexique): structure, evolution pétrologique et risques. Bulletin of Volcanology 47, 1–23.

Robin, C., Potrel, A., 1993. Multi-stage magma mixing in the precaldera series of Fuego de Colima volcano. Geofisica Internacional 32 (4), 605–615.

Robin, C., Mossand, P., Camus, G., Cantagrel, J., Gourgaud, A., Vincent, P.M., 1987. Eruptive history of the Colima volcanic complex (México). Journal of Volcanology and Geothermal Research 31, 99–113.

Robin, C., Komorowski, J., Boudal, C., Mossand, P., 1990. Mixed-magma pyroclastic surge deposits associated with debris avalanche deposits at Colima volcanoes, México. Bulletin Volcanologia 52, 391–403.

Robin, C., Camus, G., Gourgaud, A., 1991. Eruptive and magmatic cycles at Fuego de Colima volcano (México). Journal of Volcanology and Geothermal Research 45, 209–225.

Roedder, E., 1979. Origin and significance of magmatic inclusions. Bulletin of Mineralogy 102, 487–510.

Roedder, E., 1984. Fluid inclusions. Reviews in Mineralogy, vol. 12. Mineralogical Society of America, p. 646.

Roedder, E., 1992. Fluid inclusion evidence for immiscibility in magmatic differentiation. Geochemica et Cosmochemica Acta 56, 5–20.

Roggensack, K., 2001. Sizing up crystals and their melt inclusions: a new approach to crystallization studies. Earth and Planetary Science Letters 187, 221–237.

Roggensack, K., Hervig, R.L., McKnight, S.B., Williams, S.N., 1997. Explosive basaltic volcanism from Cerro Negro volcano: influence of volatiles on eruptive style. Science 277 (5332), 1639–1642.

Rutherford, M.J., Devine, J.D., 1988. The May 18, 1980, eruption of Mount St. Helens: 3. Stability and chemistry of amphibole in the magma chamber. Journal of Geophysical Research 93, 11949–11959.

Rutherford, M.J., Devine, J.D. (2003). Magmatic conditions and magma ascent as indicated by hornblende phase equilibria and reactions in the 1995–2002 Soufriere Hills magma. Journal of Petrology 44 (8), 1433–1454.

Siebe, C., Abrams, M., Macías, J.L., Obenholzner, J., 1996. Repeated volcanic disasters in preHispanic time at Popocatépetl, central Mexico: past key to the future? Geology 24 (5), 399–402.

Silver, L.A., Ihinger, P.D., Stolper, E., 1990. The influence of bulk composition on the speciation of water in silicate glasses. Contributions to Mineralogy and Petrology 104 (2), 142–162.

Sinton, C.W., Fisk, M.R., Christie, D.M., Coombs, V.L., Nielsen, R.L., 1993. Near-primary melt inclusions in anorthite phenocrysts from the Galapagos Platform. Earth and Planetary Science Letters 119 (4), 527–537.

Sisson, T.W., Grove, T.L., 1993. Experimental investigation of the role of H_2O in calc-alkaline differentiation and subduction zone magmatism. Contributions to Mineralogy and Petrology 113, 143–166.

Sisson, T.W., Layne, G.D., 1996. H_2O in basalt andesite glass inclusions from four subduction related volcanoes. Earth and Planetary Science Letters 117, 619–635.

Sisson, T.W., Grove, T.L., Coleman, D.S., 1996. Hornblende gabbro sill complex at Onion Valley, California, and a mixing origin for the Sierra Nevada batholith. Contributions to Mineralogy and Petrology 126, 81–108.

Sommer, M.A., 1977. Volatiles H_2O, CO_2 and CO in silicate melt inclusions in quartz phenocrysts from the rhyolitic Bandelier air-fall and ash-low tuff, New Mexico. Journal of Geology 85, 423–432.

Straub, S.M., Martin-Del Pozzo, A.L., 2001. The significance of phenocryst diversity in tephra from recent eruptions at Popocatépetl volcano (central México). Contributions to Mineralogy and Petrology 140, 487–510.

Thomas, J., Draper, G. (1991). Field notes for Volcán de Colima. Unpublished.

USGS Website. Melt Inclusion Page.http://wrgis.wr.usgs.gov/lowenstern/Melt%20Inc. %20Page/melt_inclusion_page.html. Adapted from: Lowenstern, J. B. (1995). Applications of silicate melt inclusions to the study of magmatic volatiles. In: Thompson, J.F.H. (Ed.), Magmas, Fluid and Ore Deposits. Mineralogical Association of Canada Short Course 23, 71–99.

Vaggelli, G., De Vivo, B., Trigila, R., 1993. Silicate-melt inclusions in recent Vesuvius lavas (1631–1944): II. Analytical chemistry. Journal of Volcanology and Geothermal Research 58 (1-4), 367–376.

Verma, S.P., 1999. Geochemistry of evolved magmas and their relationship to subduction–unrelated volcanism at the volcanic front of the central Mexican Volcanic Belt. Journal of Volcanology and Geothermal Research 93, 151–171.

Verma, S.P., 2001. Geochemical evidence for a rift-related origin of bimodal volcanism at Meseta Río San Juan, North-central Mexican Volcanic Belt. International Geology Review 43, 475–493.

Verma, S.P., Luhr, J.F., 1993. Sr–Nd–Pb isotope and trace element geochemistry of calk-alkaline andesites from Volcán Colima, Mexico. Geofiscia Internacional 32 (4), 617–631.

Vogel, T.A., Aines, R., 1996. Melt inclusions from chemically zoned ash flow sheets from the southwest Nevada Volcanic Field. Journal of Geophysical Research 101 (B3), 5591–5610.

Wallace, P.J., Carmichael, I.S.E., 1994. Petrology of Volcan Tequila, Jalisco, Mexico: disequilibrium phenocryst assemblages and evolution of the subvolcanic magma system. Contributions to Mineralogy and Petrology 117 (4), 345–361.

Wallace, P.J., Anderson, A.T., 1998. Effects of eruption and lava drainback on the H_2O contents of basaltic magmas at Kilauea Volcano. Bulletin of Volcanology 59, 327–344.

Wallace, P.J., Carmichael, I.S.E., 1999. Quaternary volcanism near the valley of México: implications for subduction zone magmatism and the effects of crustal thickness variations on primitive magma compositions. Contributions to Mineralogy and Petrology 135, 291–314.

Wardell, L.J., Kyle, P.R., Dunbar, N., Christenson, B., 2001. White Island volcano, New Zealand: carbon dioxide and sulfur dioxide emission rates and melt inclusion studies. Chemical Geology 177, 187–200.

Webster, J.D., Duffield, W.A., 1991. Volatiles and lithophile elements in Taylor Creek rhyolite: constraints from glass inclusion analysis. American Mineralogist 76, 1628–1645.

Woollard, G.P., Monges Caldera, J., 1956. Gravedad, geologia regional y estructura cortical en Mexico. Anales del Instituto de Geofisica UNAM 2, 60–112.

Yamashita, S., Kitamura, T., Kusakabe, M., 1997. Infrared spectroscopy of hydrous glasses of arc magma compositions. Geochemical Journal 31 (3), 169–174.